AGN-stimulated Cooling of Hot Gas in Elliptical Galaxies

Milena Valentini[1,2]⋆ and Fabrizio Brighenti[2]†

[1]*SISSA, via Bonomea 265, I-34136 Trieste, Italy*
[2]*Dipartimento di Fisica e Astronomia, Università di Bologna, via Ranzani 1, 40126 Bologna, Italy*

ABSTRACT

We study the impact of relatively weak AGN feedback on the interstellar medium of intermediate and massive elliptical galaxies. We find that the AGN activity, while globally heating the ISM, naturally stimulates some degree of hot gas cooling on scales of several kpc. This process generates the persistent presence of a cold ISM phase, with mass ranging between 10^4 and $\gtrsim 5 \times 10^7$ $M_\odot$, where the latter value is appropriate for group centered, massive galaxies. Widespread cooling occurs where the ratio of cooling to free-fall time before the activation of the AGN feedback satisfies $t_{\rm cool}/t_{\rm ff} \lesssim 70$, that is we find a less restrictive threshold than commonly quoted in the literature. This process helps explaining the body of observations of cold gas (both ionized and neutral/molecular) in Ellipticals and, perhaps, the residual star formation detected in many early-type galaxies. The amount and distribution of the off-center cold gas vary irregularly with time.

The cold ISM velocity field is irregular, initially sharing the (outflowing) turbulent hot gas motion. Typical velocity dispersions of the cold gas lie in the range $100 - 200$ km s^{-1}. Freshly generated cold gas often forms a cold outflow and can appear kinematically misaligned with respect to the stars.

We also follow the dust evolution in the hot and cold gas. We find that the internally generated cold ISM has a very low dust content, with representative values of the dust-to-gas ratio of $10^{-4} - 10^{-5}$. Therefore, this cold gas can escape detection in the traditional dust-absorption maps.

Key words:
galaxies: elliptical and lenticular, cD; galaxies: evolution; galaxies: ISM; galaxies: groups: general.

1 INTRODUCTION

Elliptical galaxies generally have a complex multiphase interstellar medium (ISM), which is a key component of the galactic ecosystem. The mixture of the various gas phases is usually different in early-type galaxies (ETGs) with respect to late-type systems and this, in turn, reflects on the different evolutionary pattern of morphological diverse galaxies. Reviews of hot, warm and cold gas in ETGs can be found in e.g. Caon et al. (2000); Mathews & Brighenti (2003a); Sarzi et al. (2006, 2013); Mulchaey & Jeltema (2010); Ellis & O'Sullivan (2006); Young et al. (2011); Davis et al. (2011); Serra et al. (2012). The cold ISM is often spatially extended, with irregular distribution and kinematics (Caon et al. 2000). Dust is also present in all the phases of the ISM (Temi et al. 2004, 2009; Smith et al. 2012), and the dust-to-

gas ratio can be used to track down the origin of the cold gas (see below).

A multiphase ISM is expected to keep the galaxy "alive", allowing for (perhaps tiny) episodes of star formation (SF). Indeed, a sizeable fraction of ETGs shows evidence of recent SF (Trager et al. 2000; Kaviraj et al. 2007). Therefore, a grasp on the origin and evolution of the multiphase ISM would reveal vital information on the evolution of ETGs, such as star formation history, quenching mechanism(s), the role of active galactic nuclei (AGN) feedback, black hole growth, accretion of baryons from the environment and more.

In most ETGs a significant fraction of cold gas is thought to have an external origin, as indicated by the misaligned kinematics of the cold gas (both ionized and neutral) with respect to the stars (e.g. Davis et al. 2011, and references therein). Cold gas is indeed commonly found around and bound to ETGs (Thom et al. 2012). The fate of this cold gas reservoir is still unclear, but it is likely that some

⋆ E-mail: milena.valentini@sissa.it
† E-mail: fabrizio.brighenti@unibo.it

of this low entropy gas is falling onto the galaxy and reaches the core in ≈ 1 Gyr. However, ΛCDM hydrodynamical simulations on the kinematics of accreted HI in ETGs indicate significant disagreement with respect to the observations, making the source of misaligned cold gas still an open question (Serra et al. 2014).

Some of the cold ISM certainly comes from internal processes, such as stellar mass loss or hot gas cooling (Davis et al. 2011; Werner et al. 2014; David et al. 2014). Theoretical investigations about the formation of a cold ISM phase in ETGs include Brighenti & Mathews (2002); Mathews & Brighenti (2003b); Temi et al. (2007); Parriott & Bregman (2008); McCourt et al. (2012); Gaspari et al. (2012a,b); Li & Bryan (2014); Brighenti, Mathews & Temi (2015). For massive galaxies, especially when located in high density environments, the internally produced cold gas may well dominate over the accreted one. Cavagnolo et al. (2008) and Voit et al. (2008) found that central galaxies in clusters host a multiphase gas only when the central ICM (ISM) entropy is below a threshold $kT/n^{2/3} \sim 30$ keV cm^2, providing a clear link between the presence of cold gas and the properties of the surrounding hot gas. In a recent theoretical investigation Lagos et al. (2014) argue that cooling from twisted hot gas halos results in a large fraction (~ 46 %) of ETGs with internally generated misaligned cold gas, explaining the ATLAS^{3D} observations (Davis et al. 2011).

In this paper we study the generation of a spatially extended cold gas phase in ETGs by radiative cooling of the hot halo gas. The key question is therefore if, and under which circumstances, the hot ISM can cool at large distance from the galaxy center. Multiwavelength observations often show a strong spatial correlation between X-ray and Hα images (e.g. Trinchieri et al. 1997; Goudfrooij & Trinchieri 1998; Trinchieri & Goudfrooij 2002; Temi et al. 2007; Gastaldello et al. 2009; Werner et al. 2014), implying rapid local cooling. Furthermore, the connection between cold gas, radio emission and AGN-driven X-ray disturbances (see references above, also Blanton et al. 2011) suggests the key point that spatially extended cooling has been triggered by the AGN activity. Evidently, while AGN feedback suppresses the total cooling rate with respect to standard cooling flow models (e.g. McNamara & Nulsen 2007), it also stimulates some gas condensation on scales of several kpc.

Guided by these observational results, we present here a detailed investigation of spatially extended gas cooling resulting from AGN feedback. We do not address the long term fate of the cooled gas — it can be in part accreted onto the central black hole (Gaspari et al. 2012b), it can settle in a rotating disk (Brighenti & Mathews 1996, 1997a) or it may be re-heated to the hot gas temperature by thermal conduction or other processes.

For the reasons outlined in Gaspari et al. (2012a) we consider collimated, non-relativistic outflows as the dominant feedback mechanism in local ETGs. The AGN feedback process is far more complicated than we consider here and is not appropriately understood (see, e.g. Gaspari et al. 2012a, for a discussion on the numerical limitations in simulating AGN heating in galaxies and clusters). However, for the objectives of this paper it is not necessary to accurately model the whole feedback cycle. An idealized feedback scheme as the one described in the next section is adequate enough to demonstrate the physical existence and the basic properties of widespread gas cooling in ETGs.

The thermal stability of gas in galactic or cluster cooling flows has been investigated since the discovery of the hot ISM and ICM, through both linear stability analysis and numerical simulations (see, for instance Mathews & Bregman 1978; Cowie et al. 1980; Bodo et al. 1987; Malagoli et al. 1987a; Balbus 1988a; Loewenstein 1989a; Balbus & Soker 1989a; Malagoli et al. 1990a; Hattori & Habe 1990; Reale et al. 1991; Binney et al. 2009; McCourt et al. 2012; Joung et al. 2012; Gaspari et al. 2012b; Li & Bryan 2014). However, linear stability analysis provides an incomplete understanding when strong density perturbations are present. It is quite obvious that an overdense clump of gas can cool fast and separate from the hot phase. The density contrast threshold for this localized cooling depends on the properties of the background medium and the perturbation (see Joung et al. 2012, for a recent numerical investigation). Therefore, the key astrophysical problem is to understand if such strong perturbations are naturally generated inside elliptical galaxies. As we discuss below, the answer delivered by our simulations is yes. We prefer to keep the assumptions of our models to a minimum. We do not use an *ad hoc* distributed heating to ensure global thermal equilibrium, nor we superimpose an artificial turbulent velocity field to generate density perturbations. Adopting low-power, collimated outflows as the only perturbing means of the ISM, we aim to probe the importance of AGN-stimulated cooling in ETGs in a simple yet solid way.

2   NUMERICAL PROCEDURE

The simulations have been carried out with a modified version of the eulerian code ZEUS-2D (Stone & Norman 1992), developed to include in the set of hydrodynamical equations source and sink terms describing galactic scale cooling flows. These terms include mass and energy injection by the stellar population, as described in Mathews & Brighenti (2003a). The present time type Ia supernova rate adopted here is 0.02 SNu[1]. The code has been further enhanced to deal with a second fluid representing the dust. Dust density ρ_d obeys to the equation:

$$\frac{\partial \rho_d}{\partial t} + \nabla \cdot (\rho_d\, \mathbf{u}) = \alpha_* \rho_* \,\delta_* \,-\, \dot{\rho}_{sputt} + \dot{\rho}_{growth}\,, \quad (1)$$

where $\mathbf{u}$ is the velocity of the gas, α_* the specific rate of stellar mass loss, ρ_* the stellar density and a uniform stellar dust to gas mass ratio $\delta_* = 0.01$ has been assumed. On the right hand side of equation 1, besides the stellar source term for dust, there are the sink term due to grain sputtering and the source term due to grain growth, $\dot{\rho}_{sputt}$ and $\dot{\rho}_{growth}$, respectively.

Thermal sputtering (Draine & Salpeter 1979; Tsai & Mathews 1995) rate is estimated as:

$$\dot{\rho}_{\text{sputt}} = \frac{\rho_d}{\tau_{\text{sputt}}} = n_d \,\langle \dot{m}_{\text{gr}} \rangle\,, \quad (2)$$

where $n_d = \rho_d/\langle m_{\text{gr}} \rangle$ is the number density of dust grains,

---

[1] These terms have no significant impact on our results and have been included just for consistency with previous cooling flow calculations.

$\langle \dot{m}_{\rm gr} \rangle$ is the average mass sputtering rate per grain, $\dot{m}_{\rm gr} = 4\pi a^2 \rho_{\rm gr} \dot{a}$ being the mass sputtering rate for a grain of given radius a. Here, $\rho_{\rm gr} = 3.3$ g cm^{-3} is the density of silicate grains (Temi et al. 2003), $\dot{a}$ is the rate at which the grain radius decreases (Tsai & Mathews 1995; Mathews & Brighenti 2003b) and the resulting average sputtering time is:

$$
\begin{aligned}
\tau_{\rm sputt} &= \frac{\langle m_{\rm gr} \rangle}{\langle \dot{m}_{\rm gr} \rangle} = \frac{\int_{a_{min}}^{a_{max}} a^{3-s} \, {\rm d}a}{3|\dot{a}| \int_{a_{min}}^{a_{max}} a^{2-s} \, {\rm d}a} = \frac{\langle a^3 \rangle}{3|\dot{a}| \langle a^2 \rangle} \\
&= \frac{0.03}{n_p} \left[1 + \left(\frac{2 \times 10^6}{T} \right)^{2.5} \right] \; {\rm Myr} \, .
\end{aligned}
\tag{3}
$$

In equation 3, $s = 3.5$ (Mathis et al. 1977), $a_{min} = 0.01$ μm and $a_{max} = 1$ μm [2]. Finally, $\langle a^3 \rangle = \int a^{3-s} da / \int a^{-s} da$ and similarly $\langle a^2 \rangle$.

The grain growth rate in cold and dense gas (Dwek 1988; Hirashita & Kuo 2011; Hirashita 2012; Zhukovska et al. 2008) is estimated as:

$$
\dot{\rho}_{\rm growth} \; = \; n_d \, \langle \dot{m}_{\rm gr,growth} \rangle \, ,
\tag{4}
$$

where the growth rate of each grain of mass m and radius a is $\dot{m}_{gr,growth} = \pi a^2 f n_m m_m v_m$, $f = 0.3$ being the probability that a colliding atom/metal sticks on the grain surface, n_m and $v_m \propto \sqrt{T}$ (Dwek 1998) the metal number density and thermal velocity (assuming an atomic weight $m_m/m_p = 20$). The averaged dust density growth rate is therefore:

$$
\dot{\rho}_{\rm growth} = \rho_d \frac{\langle \dot{m}_{\rm gr,growth} \rangle}{\langle m_{\rm gr} \rangle} = \frac{3}{4} \frac{\rho \rho_{\rm d}}{\rho_{\rm gr}} f v_m (0.01 - \delta) \frac{\langle a^2 \rangle}{\langle a^3 \rangle} \, ,
\tag{5}
$$

where ρ is the gas density and it has been taken into account that when the dust to gas mass ratio δ approaches the value 0.01 all the relevant metals are locked in dust grains.

Radiative cooling describing the loss of energy for X-ray emission has been included with the term $-n_i n_e \Lambda(T)$ in the thermal energy equation, where the cooling function Λ is calculated according to Sutherland & Dopita (1993), assuming solar metallicity. The cooling has been extended to temperatures lower than $T = 10^4$ K following Dalgarno & McCray (1972) and assuming a value $x = 10^{-2}$ of the fractional ionization. The cooling is truncated at $T = 50$ K. Dust-induced cooling, important for $T \gtrsim 10^6$ K for a dust-to-gas ratio $\sim 10^{-2}$, has been taken into account according to Mathews & Brighenti (2003b). We are well aware that the cooling and chemistry of cold gas is extremely complicated and our treatment for the $T < 10^4$ K gas is approximate.

The two-dimensional $z \times R$ computational domain is made up of 1100×700 zones. The resolution is $\Delta z = \Delta R = 5$ pc up to $z \times R = 5 \times 3$ kpc. The outer 100 points in both dimensions are separated by increasing distances which are the terms of a geometric progression whose common ratio is 1.095. This peculiarity of the grid allows to study the central region of the computational domain, where most of the cooling process is expected to occur, in an accurate way.

2.1 Models

We consider three models of elliptical galaxies: the *central galaxy* (thereafter *CG*), located at the center of an X-ray

bright group, the *isolated galaxy* (*IG*), an isolated, fairly massive elliptical, and the *low mass galaxy* (*LM*), an intermediate elliptical, which represents a more common member of the early-type galaxy family. The key difference between the first and the two latter models is the amount of hot gas within the galaxy, which in turn reflects on a significant difference in the cooling time profile (see Figure 4). In the *CG* most of the hot gas within 10 kpc is expected to be intragroup medium (IGM) (e.g. Brighenti & Mathews 1999), while for the *IG* and *LM* all the hot gas originates from stellar mass loss (Mathews & Loewenstein 1986; Loewenstein & Mathews 1987; Ciotti et al. 1991; Mathews & Brighenti 2003a).

2.1.1 Central Galaxy

We model the *CG* to agree with NGC 5044, the brightest galaxy in the homonymous group (see Gaspari et al. 2011b, 2012a, for further details). The gravitating mass consists of a NFW (Navarro et al. 1996) halo with virial mass $M_{\rm vir} = 4 \times 10^{13}$ M$_\odot$ and concentration $c = 8.5$, plus a de Vaucouleurs profile (Mellier & Mathez 1987) with effective radius and stellar mass $r_{\rm e} = 10$ kpc and $M_* = 3.5 \times 10^{11}$ M$_\odot$. Although inconsequential here, we also include a central black hole with mass $M_{\rm BH} = 4 \times 10^8$ M$_\odot$. Regarding the hot gas, we adopt the observed temperature profile for NGC 5044 (Buote et al. 2003, 2004; David et al. 2009) as initial temperature distribution, then we calculate the gas density profile assuming hydrostatic equilibrium, choosing the central density to approximately agree with observations. Before to activate the AGN outflow, we let the system develop a classical cooling flow, by evolving the flow for 100 Myr[3]. During this time, the initially present gas mixes with gas shed by the (old) stellar population of the galaxy[4]. The gas density and temperature profiles just before the activation of the AGN outflow are shown in Figure 1. The hot gas mass within $r = 10$ kpc is $\sim 2.6 \times 10^9$ M$_\odot$, and the bolometric X-ray luminosity within the virial radius ($r_{\rm vir} \sim 900$ kpc) is $L_{\rm X} \sim 1.5 \times 10^{43}$ erg s^{-1}. In Figure 2 it can be seen where this galaxy model is located in the B-band luminosity versus the bolometric X-ray luminosity plane for early type galaxies. As expected, it resides in the high luminosity tip of the observed $L_B - L_X$ relation (Ellis & O'Sullivan 2006), populated by massive galaxies at the center of groups or sub-clusters.
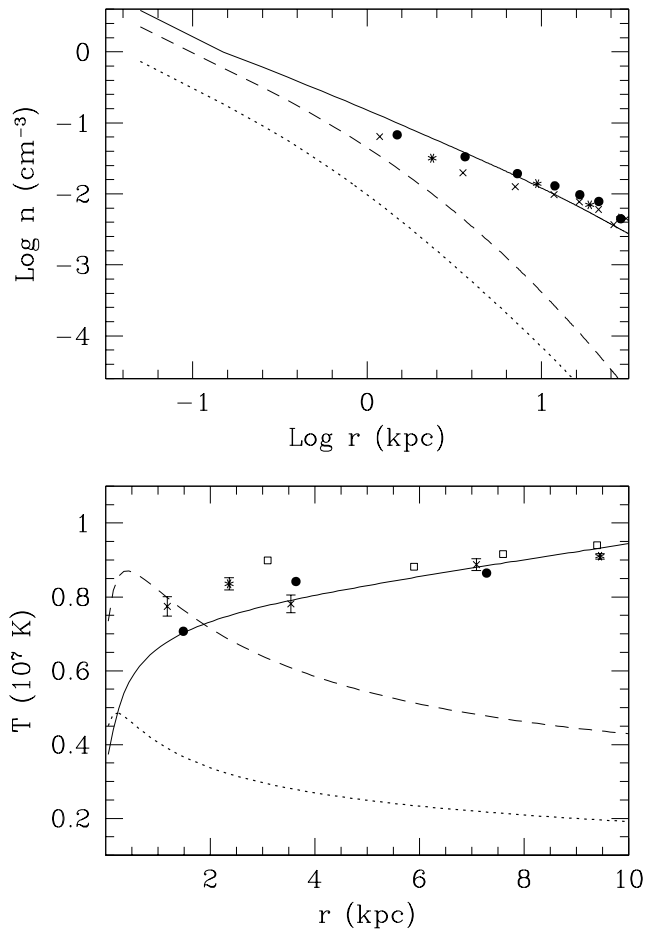
2.1.2 Isolated Galaxy

For this model, representative of massive but non central ellipticals, the stellar profile follows a de Vaucouleurs distribution, with total mass $M_* = 5 \times 10^{11}$ M$_\odot$ and effective radius $r_{\rm e} = 6$ kpc. The dark halo has a NFW profile with virial mass $M_{\rm vir} = 10^{13}$ M$_\odot$ and concentration 10.0.

[2] We checked that these values of minimum and maximum grain size do not affect our results.

[3] This has a negligible effect on the results presented in the following. We decided to kick off the AGN feedback from a pure cooling flow just to be consistent with the *IG* and *LM* models.

[4] We refer the reader to Mathews & Brighenti (2003a) for the hydrodynamical equations solved here and the relevant source terms for mass and energy.

Figure 1. *Upper panel:* Density profile just before the outflow activation for the central galaxy (solid line), the isolated galaxy (dashed line) and the low mass galaxy (dotted line). The points represent data for NGC 5044 taken from Buote et al. (2003, 2004); David et al. (2009). *Bottom panel:* initial (3D) temperature profiles for the central galaxy (solid line), the isolated galaxy (dashed line) and the low mass galaxy (dotted line). Data points for NGC 5044 are taken from Buote et al. (2003, 2004); David et al. (2009).

The initial ISM is generated by evolving a classic cooling flow for 1 Gyr (the choice of this time is arbitrary and has no consequence on the results, since the flow reaches a quasi-steady state after ~ 100 Myr). The ISM entirely builds from the mass loss from the stellar population (e.g. Loewenstein & Mathews 1987; Mathews & Brighenti 2003a). Just before the AGN outburst, the hot ISM mass within 10 kpc is $\sim 1.9 \times 10^8$ M$_\odot$, the X-ray bolometric luminosity being $L_x \sim 1.2 \times 10^{41}$ erg s^{-1}. Figure 2 shows that this model occupies an intermediate and uninteresting place in the $L_B - L_X$ diagram. The initial gas density and temperature profiles are shown in Figure 1 as dashed lines. Notice as pure cooling flows in elliptical galaxies show an overall negative temperature gradient, because of the central steep potential well and the resulting compressional heating.
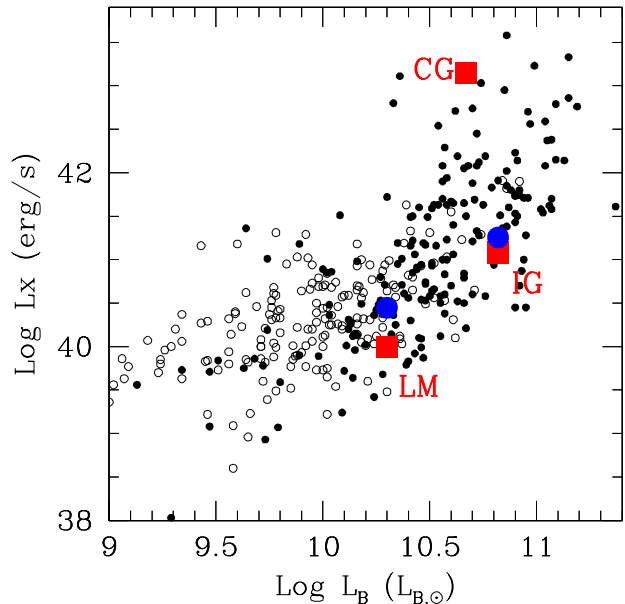

Figure 2. $L_B - L_X$ diagram for the elliptical galaxies sample of Ellis & O'Sullivan (2006). Filled circle represent galaxies with detected X-ray emission; open circles are used for upper limits. The location of our models, just before the AGN activation, is marked with the red squares when only the X-ray luminosity of the hot gas is considered. Big blue dots individuate the models when the contribution of the low mass X-ray binaries is added (Kim & Fabbiano 2004).

2.1.3   Low Mass Galaxy

This model is a scaled down version of the *IG* described above. The stellar mass is now $M_* = 1.5 \times 10^{11}$ M$_\odot$ and the effective radius $r_e = 3.16$ kpc, a value which agrees with the magnitude-r_e relation (Faber et al. 1997). The NFW dark halo has a virial mass $M_{vir} = 1.5 \times 10^{12}$ M$_\odot$ and concentration 11.9. The mass of hot gas within $r < 10$ kpc is only $\sim 3.4 \times 10^7$ M$_\odot$ ($\sim 1.15 \times 10^7$ M$_\odot$ within r_e), with a X-ray (bolometric) luminosity $L_x \sim 10^{40}$ erg s^{-1}, which places this model within the lower envelope of the $L_B - L_X$ relation.

As common in intermediate and low mass ellipticals, only the gas in the inner region is inflowing, while the ISM at larger radii forms a subsonic outflow, powered by the SNIa (e.g. Mathews & Baker 1971; Mathews & Brighenti 2003a). For the assumed SNIa rate (0.02 SNu), the transition between inflow and outflow is located at $r \sim 2$ kpc. We note that for this relatively small galaxy the properties of the ISM are quite sensitive to the SN heating. Doubling the SNIa rate results in a global outflow (but the inner ~ 200 pc), with velocity increasing almost linearly from ~ 0 at 200 pc to ~ 60 km s^{-1} at 3 kpc. The hot gas mass (within 10 kpc) is reduced to 1.9×10^7 M$_\odot$, while the X-ray luminosity drops to a very small value of 1.8×10^{39} erg s^{-1} (see Mathews & Brighenti (2003a) for more details on the effect of the SNIa rate on the gas flow in elliptical galaxies).
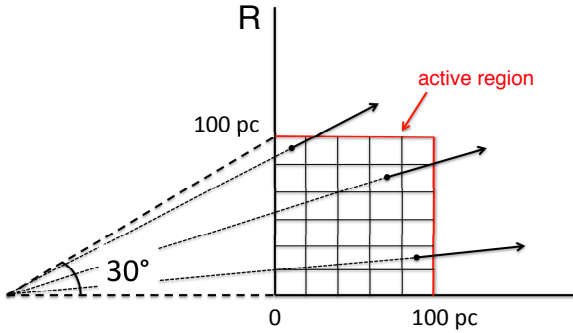
Figure 3. Scheme showing the method we chose to implement a conical outflow (see text). The inner corner of the 2D cylindrical grid, with the 100×100 pc^2 active region highlighted, is represented. We note that in the code the z and R components of the velocity are located on different positions (see Stone & Norman 1992). Here we show the velocity vectors originating from the grid center just for illustrative purposes.

2.2 Modeling the outflow

2.2.1 Single event

A subrelativistic and massive outflow (Brighenti & Mathews 2006; Gaspari et al. 2012a) which lasts 2 Myr (e.g. Fabian 2012) is our single event AGN mechanical outburst. The outflow energy injection is simulated dispensing velocity to the gas located in a box of $(R \times z) = (100 \times 100)$ pc. This *active region* is the inner corner of the computational domain, near the origin of the R and z-axis[5].

The number of cells by which resolve the interior of the jet has been chosen arbitrarily, the reasonable assumption is that the physics of the outflow does not influence the AGN feedback effects on kpc scale-length and the IGM global properties.

The outflow velocity is given to the cells of the active region while the AGN is switched on, this energy input representing a spatially localized source term in the hydrodynamical equation of momentum. The velocity is given setting its module and defining a way for describing the components along R and z axes. We simulate both cylindrical and conical outflows, although we will focus mainly on the latter case. Cylindrical outflows have been simulated by equating the z-component of the velocity to the velocity module and setting the R-component equal to zero in all the aforementioned zones. On the other hand, for conical outflows we set the velocity vectors as illustrated in Figure 3. At any given grid point the velocity is radially directed, with the center located at $(z, R) = (0, -100 \text{ pc/tg}(30^\circ))$. The results are quite insensitive to the exact method of implementing a conical outflow.

All the models have been evolved for 50 Myr, in order to investigate the short term evolution of a single AGN outburst. Each performed simulation was given a name: the identifying convention encodes the model of galaxy and both the shape and the velocity in km/s of the outflow. For in-

stance, model *IG4000* refers to the conical outflow with $v_{jet} = 4000$ km s^{-1} activated in the isolated galaxy.

2.2.2 AGN feedback: recurrent outbursts

In these models we consider the whole AGN feedback cycle, where the gas cools and accretes on the central black hole, triggering an AGN outburst which heats the ISM. When the gas cools in the central region, the cycle is assumed to start again. Needless to say, the physics of AGN feedback is very complex and poorly known. We have no pretension to provide a self-consistent model here, we just need a simple scheme to set off outflows intermittently, in order to mimic the dynamical — sometime violent — evolution of the ISM in elliptical galaxies. We thus employ a simplified version of the feedback scheme used elsewhere (e.g. Brighenti & Mathews 2006; Gaspari et al. 2012a). Although this feedback is not fully self-regulated, the modeled outflows reproduce reasonable energies and powers (see Section 8).

The adopted recipe has two main ingredients: the way of numerically describing the outflow and its activation timing. We adopted a simple method in which the mechanical feedback activation is triggered by the presence of cooling gas in the innermost region ($r \leqslant 100$ pc) of the simulated galaxy. This assumption mimics the so-called cold accretion idea (e.g. Gaspari et al. 2012b, and references therein): AGN outflows are fed by accretion of gas cooled out of the hot ISM, which accretes onto the central black hole.

After several numerical experiments, we decided to adopt a *dropout* term $-q(T)\rho/t_{cool}$, with $q(T) = q_0 \exp[-(T/T_c)^2]$, (Brighenti & Mathews 2002) in the continuity equation to individuate and remove from the grid gas currently cooling to low temperatures. When gas dropout within $r \leqslant 100$ pc occurs (at least 1 $M_\odot$ in one timestep), the outflow is set off. We choose $q_0 = 2$ and $T_c = 5 \times 10^5$ K to describe $q(T)$, although the results are insensitive to the exact values of these parameters. This dropout method might result unpalatable and contrived, but has been shown to provide realistic estimates for cooled gas masses, limiting the effect of numerical overcooling over the traditional approach (see Brighenti & Mathews (2002), Brighenti, Mathews & Temi (2015) and the Appendix). Beside rectifying the numerical overcooling problem, there is an even more crucial reason to prefer the dropout technique. In order to calculate the genuine cooling rate at large distances from the center, it is preferable to avoid the presence of cold gas in the inner region, which would be ejected through an AGN outflow possibly reaching the off-center region and mixing with the freshly cooled hot gas.

We note that we use the dropout term only near the center of the system (for $r < 500$ pc), so that the off-center gas cooling (see below) is calculated in the standard way, that is letting the gas cooling to low temperatures and keeping it on the numerical grid, although this is know to cause spurious overcooling (see Appendix).

Once the outburst has been activated, the gas which resides in the inner region defined by $R < 100$, $z < 100$ pc is given a constant velocity as long as the condition on the presence of dropping out gas in $r \leqslant 100$ pc is met.

All the models consider a sequence of conical outflows, their opening angle being $\theta = 30^\circ$, and evolve up to 50 Myr. Models of recurrent feedback (*FB*) were given a name which

---

[5] Numerical experiments show that injecting the kinetic energy from a nozzle along the inner boundary conditions at $z = 0$ does not change the results.

shows the model of galaxy and the velocity in km/s of the outflows, for instance *CG-FB2000*.

3   COOLING AND TIMESCALES

Here we briefly discuss the relevant timescales for thermal instability for our three models. It is well known that linear (infinitesimal) perturbations in the central regions of ETGs and galaxy clusters are generally stable in the pure hydrodynamical case (e.g. Malagoli et al. 1987b; Balbus 1988b; Loewenstein 1989b; Balbus & Soker 1989b; Malagoli et al. 1990b; Binney et al. 2009). In fact, slightly overdense fluid elements oscillates at the Brunt-Väsäilä frequency $\omega_{BV} = 2\pi/\tau_{BV}$, where usually the oscillation period $\tau_{BV} \ll t_{cool}$. The oscillation center of the perturbation slowly sinks toward the center of the system, in a time only slightly shorter than the flow time of unperturbed gas.

However, the linear stability analysis is of limited use, as in realistic galactic environments violent dynamical processes are expected to generate perturbations of finite amplitude. Indeed, X-ray images of cool cores clearly show large variations of gas density on all scales probed by current telescopes.

Brighenti & Mathews (2002) have shown that spatially extended gas cooling in a cool core can happen when the hot gas is perturbed by the action of AGN feedback heating. Brighenti & Mathews (2002) found that localized nonlinear perturbations form in regions of converging flow and are able to cool without undergoing oscillations. Recently, McCourt et al. (2012); Sharma et al. (2012); Gaspari et al. (2012b); Singh & Sharma (2015) have studied in detail the cooling process in galaxy cluster cores perturbed by AGN feedback (see also Gaspari et al. 2011a). They provide a heuristic criterion for the onset of off-center thermal instability: the ICM undergoes widespread cooling when stirred by AGN feedback if $t_{cool}/t_{ff} \lesssim 10$, with the free fall time $t_{ff} \sim t_{dyn} = (2r/g)^{1/2}$, g being the local gravitational acceleration. Joung et al. (2012) investigated the evolution of nonlinear perturbations in the Galactic halo and found that for $t_{cool}/t_{acc} \lesssim 1$ the "cloud" cools before being disrupted by hydrodynamical instabilities. Here $t_{acc} = c_s/g$, which is similar to t_{ff}.

In Figure 4 we show the ratios t_{cool}/t_{acc} and t_{cool}/t_{ff} for our three systems, at the time just before the AGN activation. For the *CG* model the instability criterion $t_{cool}/t_{ff} \lesssim 10$ is met for $r \lesssim 6$ kpc, while for *IG* and *LM* no unstable region exists outside the galactic core $r \lesssim 100$ pc, according to Sharma et al. (2012).

However, in the following we show that the commonly adopted instability criterion is too restrictive. We find that extended cooling within elliptical galaxies occurs for $t_{cool}/t_{ff} \lesssim 70$ for realistic, recurrent, gentle AGN outbursts. We note that the empirical entropy criterion for star formation and multiphase gas in galaxy clusters cool cores, $K = kT/n^{2/3} \lesssim 30$ keV cm^2 (Voit et al. 2008; Cavagnolo et al. 2008) describes more accurately the spatial extent of the region where cooling happens. For the profiles shown in Figure 1 we find that the radius where $K = 30$ keV cm^2 is 17, 5.4, 3.6 kpc for model *CG, IG* and *LM*, respectively. These numbers compare well with the maximum size of the region where cooling occurs.

4   SPATIALLY EXTENDED COOLING: SINGLE AGN OUTFLOW

Below we analize the dynamics and the off-center cooling process triggered by a single AGN outburst. We focus here on the conical outflows, the cylindrical ones giving qualitatively similar results. This idealized case will be used to better understand the physical nature of the non-linear density perturbations which lead to widespread cooling. We expect that in a more chaotic and realistic ISM, perturbed by the intermittent action of AGN feedback, extended cooling would be facilitated. This is the subject of Section 5. In the following we focus on the gas that cools in the "off-center region" defined as: $z > 500$ pc, $R > 150$ pc. We exclude the region near the symmetry z-axis because the 2D cylindrical grid used in our simulations might lead in spurious enhanced cooling along the axis. Indeed, the formation of cold gas along the jet axis is a common result of our simulations. This is physically reasonable because when the cavities generated by the AGN jets move buoyantly toward larger distances, they trigger a vortex flow around them, which compresses the hot gas toward the z-axis, significantly lowering the local cooling time (see also Mathews & Brighenti (2008); Revaz et al. (2008); Brighenti, Mathews & Temi(2015)). Preliminary 3D calculations verify the formation of the $z-$axis cold filament (C. Melioli, in preparation), but we still prefer to be conservative in this work and focus on the region far from the symmetry axis for most of our analysis.

We also neglect the gas which cools at the very center. The suppression of the total cooling rate in galaxies and clusters relates to the so-called cooling flow problem (McNamara & Nulsen 2007) and will not be discussed here. For calculations about AGN heating in ellipticals see Gaspari et al. (e.g. 2012a), which use a similar feedback scheme.

4.1   AGN-cooling in the Central Galaxy

In the top panel, central column of Figure 5 we show the time evolution of the cold gas mass located off-center ($z > 500$ pc, $R > 150$ pc), for the single conical outflow models. Times are measured since the activation of the outflow. For the *CG*, the three models with $v_{jet} = 2000, 4000, 8000$ km s^{-1} are able to cool a substantial amount of gas, $10^4 - 10^7$ M$_\odot$, at large distances from the center. A weak trend with v_{jet} is evident from Figure 5: the larger is v_{jet}, the larger is the mass cooled off-center. As already found in Brighenti & Mathews (2002), the AGN feedback generates non-linear, almost isobaric perturbations in regions of sustained compression, which trigger intermittent and widespread cooling throughout the region with $t_{cool}/t_{ff} \lesssim 10$. Because of the large overdensities formed in converging flows, it seems improper to describe this cooling process as a thermal instability. This agrees with recent studies of cooling in galaxy clusters by McCourt et al. (2012); Gaspari et al. (2012b). Contrary to these latter works, however, we do not include an artificial source of turbulence nor a distributed source of heating. Generally, the region over which cooling occurs is more extended when the power of the outflow is larger.

Interestingly, cooling can occur long after the AGN outflow ceases (see also Brighenti, Mathews & Temi, 2015). For instance, for models *CG4000* and *CG8000* off-center cooling episodes happen at $t \sim 35$ Myr and $t \sim 50$ Myr, respectively,
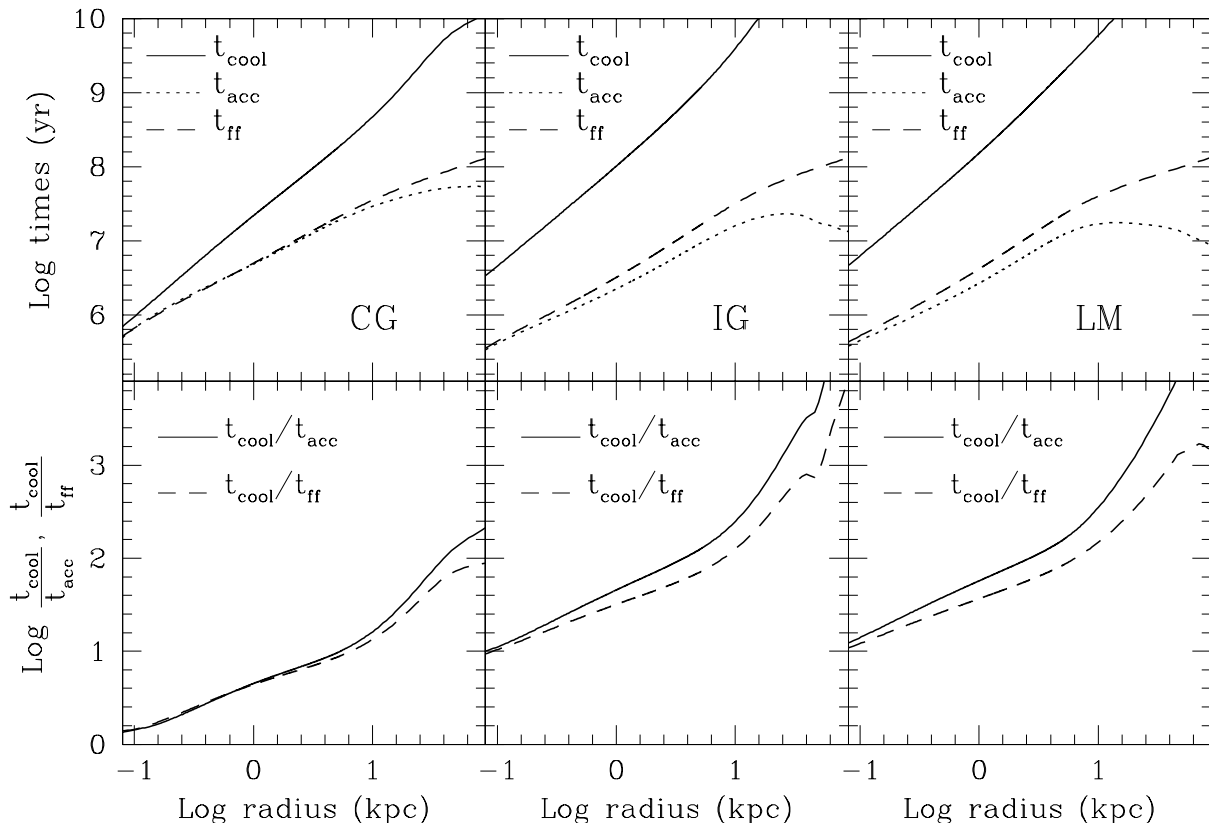
Figure 4. *Upper panels:* Cooling time, acceleration time and free fall time (see definitions in the text) just before the AGN outburst, for the *CG* (left), the *IG* (middle) and *LM* (right). *Bottom panels:* ratios of relevant timescales.

while the outflow terminated at $t = 2$ Myr. At these times, usually no sign of the AGN feedback (cavities, shocks) would be detected with X-ray observations. Nevertheless, subsonic motion with velocity up to $\sim 1/2$ of the sound speed is still present in localized regions, especially in form of relatively large eddies with typical size ~ 0.5 kpc. We note that these features are well resolved in our simulations with $\sim 50-100$ grid points. When exceptionally large eddies are present in the inner region of the galaxy, they appear as weak X-ray cavities. This happens infrequently in our simulations, with large outflow velocities and earlier times making this event more likely.

The spatial distribution of the cold gas in the off-center region at several times, for models *CG4000* and *CG8000*, is displayed in Figure 6. The cold blobs generally arise in a region close to the outflow symmetry axis ($R \lesssim 1$ kpc) and for $z \lesssim 10$ kpc. The cold gas is arranged in a large number of small clouds (actually, toroidal structures, given the imposed 2D cylindrical symmetry), generally few 10s pc in size. As expected (see Koyama & Inutsuka 2004) this is close to our numerical resolution ($\Delta R = \Delta z = 5$ pc), with the unfortunate implication that the evolution of the cold clouds may be subject to serious numerical errors. We address some of the numerical problems, such as overcooling, in the Appendix. The off-center cooling process starts in a very localized fashion, usually in just one or few zones (see, for example, the top-left panel in Figure 6). This is true for

every resolution adopted in our numerical experiments. Calculations using coarse resolution might be grossly in error.

Using a tracer passively advected with the flow, we are able to track down the original location of the cooling gas. We find that most of the cold gas found off-center comes from the inner region ($r \lesssim 1$ kpc), where the entropy is lower. This confirms the results by Li & Bryan (2014). Because the ISM (iron) abundance peaks in the center, it also follows that the metallicity of the cold gas is somewhat higher than the one of the surrounding hot gas.

In Figure 5 we also show, in the central row, the evolution of the cold gas mass in the region $r = \sqrt{R^2 + z^2} > 500$ pc (that is, we include here the cold filament along the $z-$axis) and the total cold gas (bottom panels). The mass in the filament forming in the wake of the outflow lies in the range $M_{\rm fil} \sim 10^4 - 10^6$ M$_\odot$[6], although these values must be confirmed by high resolution 3D simulations. The time evolution of the total cold gas mass shows that the single AGN outburst is unable to significantly suppress the cooling rate with respect to the pure coling flow scenario. Only for the *CG8000* model the AGN outflow temporarily reduces the cooling rate by a factor of ~ 2.5 for a time ~ 15 Myr, after which the system recovers the standard cooling rate, $\dot{M} \sim 10$ M$_\odot$ yr^{-1}.

[6] Note that here and in the following we consider only the $z > 0$ volume.
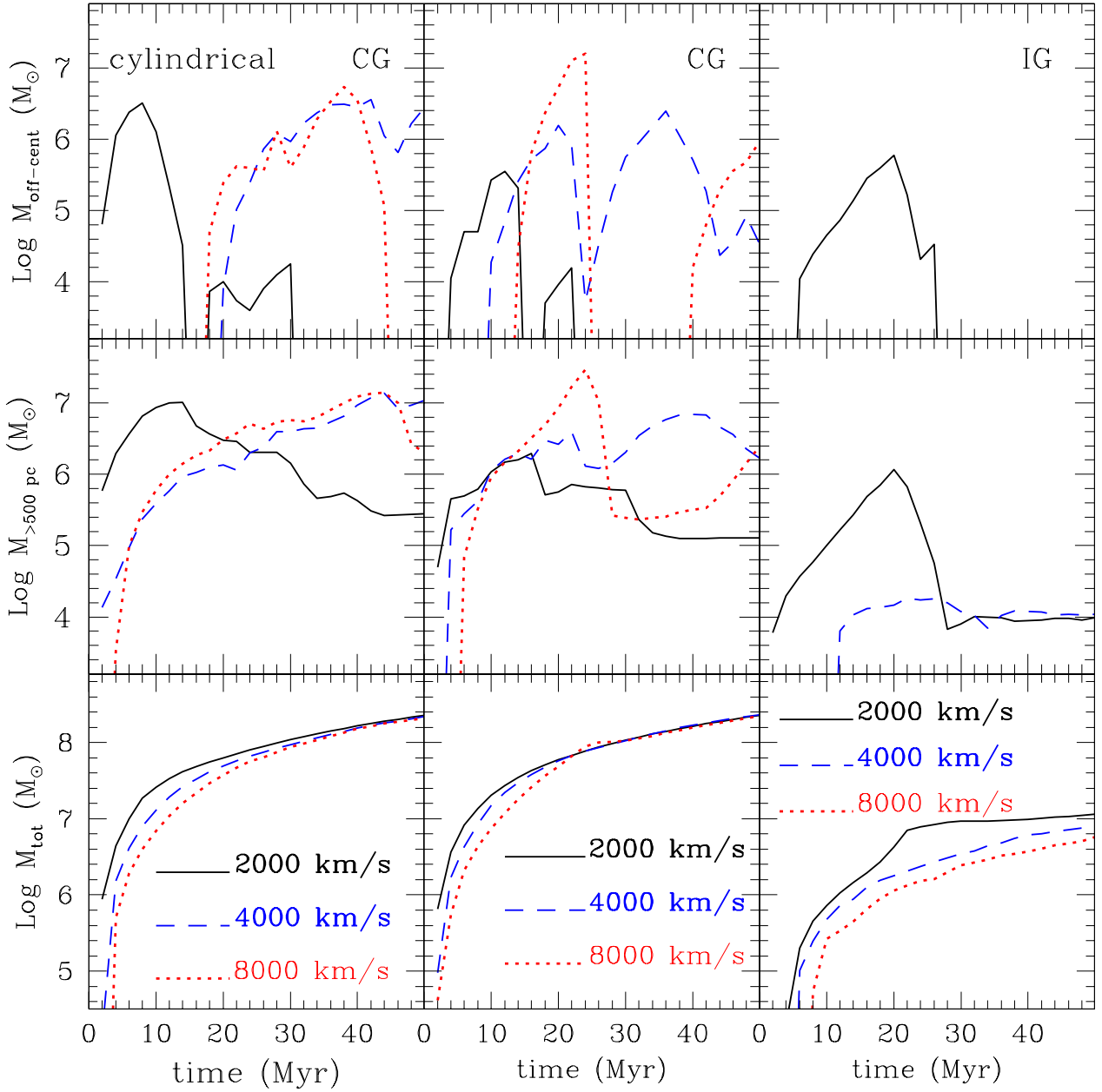
Figure 5. *Upper left panel:* Time evolution of the cold gas mass in the off-center region ($R > 150$ pc, $z > 500$ pc), for *CG* models with cylindrical jets *CGcyl2000*, *CGcyl4000* and *CGcyl8000*. Here and in the following, times are measured since the start of the AGN aoutflow. *Middle left panel:* as above for the total cold gas mass in the region $r > 500$ pc, which includes the filament along the $z-$axis. *Lower left panel:* same for the total cold gas mass, most of which is located at the very center of the galaxy ($r < 300$ pc). *Central panels:* same as left panels but for the *CG* galaxy with conical jets (30 degrees) models *CG2000*, *CG4000* and *CG8000*. *Right panels:* same as central panels but for the isolated galaxy.

4.1.1 Cylindrical outflows

We have also calculated several models with cylindrical outflows, in which the velocity is directed along the $z-$axis. The time evolution of the cold gas mass for the models with jet velocity 2000, 4000 and 8000 km s^{-1} is shown in the first column of Figure 5. The results are qualitatively similar to the conical outflows, with a tendency to generate more off-center cold gas. The reason is that cylindrical outflows are less efficient to distribute their kinetic energy in the inner region of

the galaxy, therefore a larger volume of the system hosts an almost unperturbed cooling flow. Also, it is well known that conical AGN outflows get collimated by the hot gas pressure as they propagate outward, becoming effectively cylindrical at some distance from the center (cfr. Brighenti & Mathews 2006). Given the similarity of models with conical and cylindrical outflows (and the uncertainties about real AGN outflows), in the following we limit the discussion to conical jets.
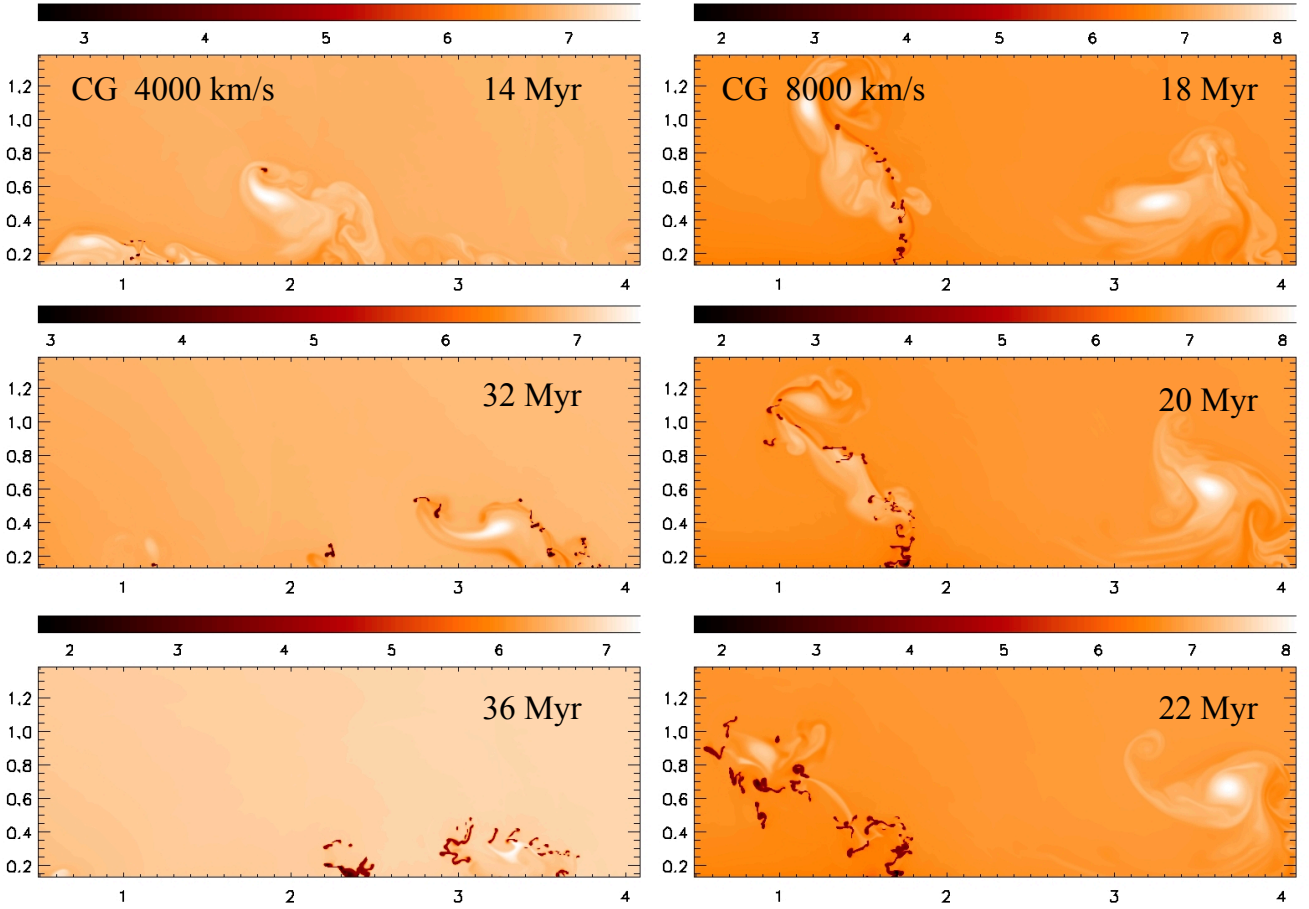
Figure 6. *Left column:* temperature map for model *CG4000* at three different times: $t = 14, 32, 36$ Myr, from top to bottom. The z-axis is horizontal, the R-axis is vertical. Units are kpc. Time is measured since the switch on of the AGN outflow (which lasts 2 Myr). *Right column:* same for model *CG8000*. The temperature is shown at $t = 18, 20, 22$ Myr, to follow a strong cooling episode. Notice that the color scale differs for every panel.

4.2 AGN cooling in the Isolated Galaxy

As pointed out in Section 3, the fundamental difference between the *IG* and the *CG* models is that in the former the whole hot ISM is generated by the stellar mass loss of the galactic (old) stellar population. Therefore, the mass and the average density of the hot gas is much lower than in the *CG* case. As a result, the ratio $t_{\rm cool}/t_{\rm acc}$ for the *IG* is everywhere larger by a factor of $\gtrsim 10$ than for the *CG* (see Figure 4). According to the criterion by Sharma et al. (2012) and McCourt et al. (2012) we should not expect spatially extended cooling for this model. This conjecture does not pass the test of our simulations. In fact the model *IG2000* gives rise a substantial mass of cold gas at $t \sim 5 - 25$ Myr (top-right panel of Figure 5). We will see below that in case of repeated AGN outbursts, even moderate outflows with velocity of 1000 km s^{-1} trigger significant off-center cooling. The spatial map of the cold gas for *IG2000* is shown in Figure 7. The off-center cooling process initiates at $t \sim 5$ Myr, with small cold blobs forming at $(R, z) \sim (0.2, 2)$ kpc and $(R, z) \sim (0.4, 2.1)$ kpc, where the time ratio $t_{\rm cool}/t_{\rm acc} \sim 60$,

just before the AGN activation[7]. As time goes by, more gas cools and moves away from the original formation location. At later times, as shown in Figure 7, a multitude of cold clumps can be found for $(R, z) \lesssim (0.7, 2.5)$ kpc. As for the *CG* simulation, the emergence of the off-center cooling depends on two effects. First, the outflow transports (low entropy) gas initially at the center to larger radii (see also Li & Bryan 2014). Second, the dynamical evolution of the AGN outflow generates regions of sustained compression (where $\nabla \cdot v < 0$), which gives rise to high contrast density inhomogeneities.

As in the model *CG*, a massive cold filament is created along the axis of the jet, with mass $\sim 10^4$ M$_\odot$, for models *IG2000* and *IG4000*. No gas cools instead for $r > 500$ pc in the case of the more powerful model *IG8000* (middle-right panel of Figure 5). Evidently, the AGN heating is strong enough to completely suppress off-center cooling, at least for the timespan probed by our simulation.

---

[7] Just before the time of the first off-center cooling episode, the ratio $t_{\rm cool}/t_{\rm acc}$ near the cooling region has values in the range [20-50]. This is due to the advection of low entropy material from the center by the AGN outflow.
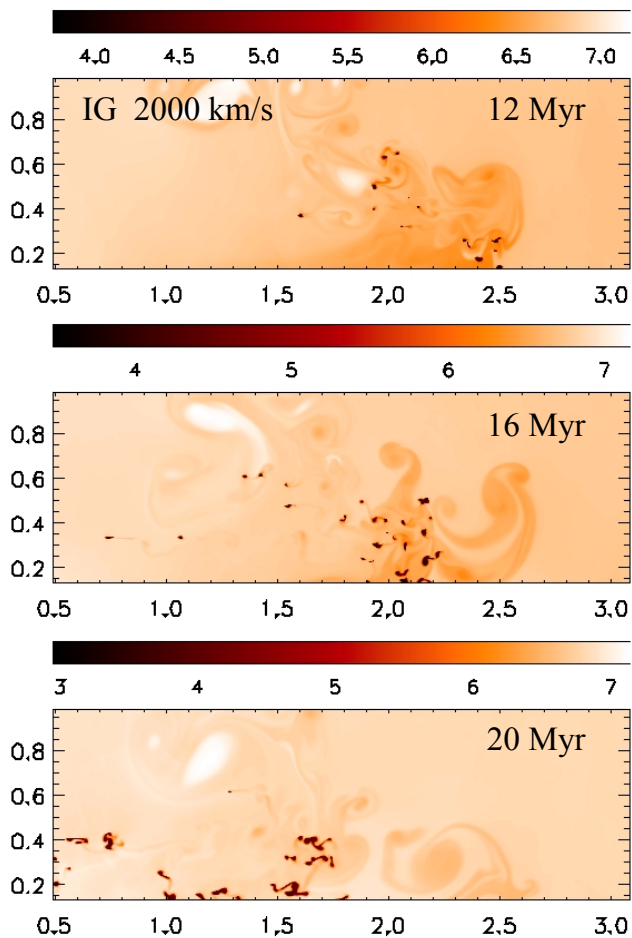
Figure 7. Temperature maps for the isolated galaxy "single event" and $v_{\mathrm{jet}} = 2000$ km s^{-1}. Top panel: $t = 12$ Myr; middle panel: $t = 16$ Myr; bottom panel: $t = 20$ Myr. The z-axis is horizontal, the R-axis is vertical. Units are kpc. Notice that the color scale differs for every panel.

We notice that the average total cooling rate in the 50 Myr following the AGN outflow, for models *IG1000, IG2000, IG4000* and *IG8000*, is 0.5, 0.45, 0.32, 0.24 M$_\odot$ yr^{-1} (see bottom-right panel of Figure 5 - model *IG1000* is not shown). These values reflect the (temporarily) suppression of cooling due to AGN activity, being the cooling rate of the pure cooling flow model $\dot{M}_{\mathrm{cool}} \sim 0.8$ M$_\odot$ yr^{-1} .

4.3 AGN cooling in the Low Mass Galaxy

We describe only very briefly the single outflow models for the low mass galaxy. Because of the lower hot ISM density, widespread cooling is less efficient for this system. However, we shall see below (Section 5.3) that when repeated AGN events are considered, even the *LM* model undergoes significant off-center cooling.

For the single outflow experiments, we find that only *LM2000* shows extended cooling, for $t \sim 10 - 25$ Myr, when $\sim 10^3 - 3 \times 10^3$ M$_\odot$ are present in the off-center region. Few small blobs develop at $z \sim 4$, $R \sim 0.5$ kpc. As usual, a cold

filament also forms along the $z-$axis, with mass $\sim 3 \times 10^3$ M$_\odot$.

5 SPATIALLY EXTENDED COOLING: AGN FEEDBACK

The models presented in Section 4 showed that the dynamical interaction of a single AGN-driven outflow with a smooth and regular ISM generates density (entropy) perturbations which lead to (sometime recurrent) widespread gas cooling. Understanding these idealized calculations has been preparatory to the study of the more realistic problem of repeated AGN outbursts, the subject of this Section.

The intuitive expectation is that in an ISM continuosly stirred by the AGN feedback activity the generation of non-linear perturbations is facilitated, with the result of more intense cooling episodes. This is indeed what the simulations presented below show.

5.1 Feedback in Central Galaxies

In Figure 9 we show the off-center temperature maps for the feedback models of the *CG* galaxy, with outflow velocities of 2000, 4000 and 8000 km s^{-1}. The dark spots in every panel indicate gas cooled to $T < 10^4$ K. In Figure 8 the mass of cold gas in the various regions, as defined in the previous sections, is shown for most models. The first result revealed by these images is that a persistent cold ISM phase is naturally present, regardless on the feedback details. Of particular interest is model *CG-FB16000* — with the fastest outflows among our simulations — shown in Figure 8 with the magenta dot-dashed line. In this system the AGN heating is strong enough to suppress almost completely the cooling at the center of the galaxy (where all the cooling in the classic cooling flow picture would occur). Despite that, a strong off-center cooling episode happens at $t \sim 24$ Myr and generates a total cold gas mass $M_{blob} \sim 1.5 \times 10^8$ M$_\odot$.

The network of blobs and filaments occupies a region typically few kpc in size and has mass $M_{\mathrm{blob}} \sim 10^6 - 10^7$ M$_\odot$. We are not in the position to calculate the fraction of this gas in molecular, neutral or photoionized state. It is likely, however, that all these components are simultaneously present (see our Discussion below), as supported by observations (e.g. Werner et al. 2014; David et al. 2014). The spatial distribution of the cold gas generally correlates with the direction of the outflows and with the disturbances induced in the hot gas. It is worth noting that the brightness of warm gas clumps is expected to decrease with the distance from the center, in pace with the decrease of the pressure. The aspect and amount of the AGN-triggered cold phase are in broad agreement with warm/cold gas observations in massive ellipticals/galaxy groups (Caon et al. 2000; Werner et al. 2014). We believe that this is the most robust and relevant result of our simulations. The velocity structure of the spatially extended cold phase is discussed in Section 7.1.

The filament of cold gas forming along the $z-$axis is always present in the *CG* simulations, with mass which varies between few 10^5 to few 10^7 M$_\odot$. The filament has often a clumpy appearance, with density variations within it of 2

orders of magnitude. The velocity of the cold gas is generally negative (especially at late times) with typical values of $100 - 200$ km s^{-1}, but outflowing portions of the filament are also present.

The physics of a multiphase ISM and the interaction between the phases is very complex, a process poorly understood even in our own Galaxy (e.g. Cox 2005), and we have no chance to give a consistent description here. As for the single outflow case, the cold material in our feedback simulations condenses in very small structures, usually few numerical zones in size. Resolution tests indicate that this is true even when the cell size is reduced by a factor of 5 (that is, adopting $\Delta R = \Delta z = 1$ pc). The volume filling factor in the central region where cold gas is found is always very small, usually less than 2-3%. Off-center cold gas usually spans temperatures in the range $10^3 - 10^4$ K, with only a few percent undergoing cooling below 100 K.

Initially, the cold blobs share the same turbulent velocity field of the hot gas out of which they form. Then, they start to fall toward the center of the system, which is reached in about a dynamical time ($\sim 10^7$ yr); this is the typical lifetime of an off-center cloud or filament.

5.2 Feedback in the Isolated Galaxy

The isolated galaxy, although more optically luminous than the *CG*, has a much lower amount of hot ISM. As discussed earlier on, this leads to a longer t_{cool} and a larger t_{cool}/t_{acc}. Correspondingly, the entropy is higher. However, this only slightly hinders the spatially cooling process (see also Section 4.2). We find that both models *IG-FB1000* and *IG-FB2000* generate an extended cold ISM phase, whose physical properties vary in time (see Figures 8 and 10). Total masses of cold gas $M_{cold} \sim 10^5 - 10^6$ M$_\odot$ are common in the off-center region ($R > 500$ pc, $z > 150$ pc). For model *IG-FB4000* only little gas cools in this volume, $M_{cold} \sim 3.8 \times 10^3$ M$_\odot$, and there is only one episode of extended cooling at $t \sim 30$ Myr. Of course it is possible, perhaps likely, that more gas would condense at times > 50 Myr. We did not calculate a feedback model for the *IG* with $v_{jet} = 8000$ km s^{-1}, but it seems plausible that recurrent outflows with such a velocity prevent off-center cooling completely, as the single outflow does for the *IG8000* model (see Section 4.2).

The cold gas mass in the $z-$axis filament is comparable with that in the off-center blobs, varying between zero and $\sim 7 \times 10^5$ M$_\odot$ in models *IG-FB1000* and *IG-FB2000*, while for *IG-FB4000* it reaches $\sim 7 \times 10^4$ M$_\odot$ at its maximum (cfr. top and bottom panels in Figure 8).

5.3 Feedback in the Low Mass Galaxy

Results for this model, which has an optical luminosity close to the L^* parameter of the luminosity function, are relevant for a large number of normal elliptical galaxies. Before the onset of the AGN, the (hot) ISM mass within the effective radius is $\sim 1.2 \times 10^7$ M$_\odot$; within $r \sim 2$ kpc the ISM is slowly inflowing as in the classical cooling flow theory, while at larger radii the SNIa heating generates a highly subsonic outflow, with average velocity $v \sim 10$ km s^{-1}. Is interesting that while gas cooling occurs also where $t_{cool}/t_{acc} \gg 10$, it is however limited to the ISM inflowing region ($r \lesssim 2$ kpc,

Figure 10), within which the initial ISM mass is $\sim 6.9 \times 10^6$ M$_\odot$. We also calculated few models with a higher SNIa rate (and therefore a smaller or no inflowing region, although the outflow velocity is still very subsonic) to test the reasonable hypothesis that global inflow (except for the outflow region, which occupy a small volume of the system) is a necessary condition for widespread cooling. Clearly, non linear density perturbations moving outward, toward lower pressure regions, would expand, lengthening t_{cool} and delaying or frustrating the cooling process. In these "windy" galaxies we find that no gas cools[8].

In Figure 8, right column, the time evolution of cold gas mass in the off-center region and in the $r > 500$ pc region is plotted. For models *LM-FB1000* and *LM-FB2000* an extended cold ISM phase naturally forms within $r \lesssim 1$ ($r \lesssim 2$) kpc for *LM-FB1000* (*LM-FB2000*), again in an elongated region around the $z-$axis. For the high outflow velocity model *LM-FB4000* no gas is able to cool. In this case the AGN heating offsets radiative cooling for the (short) time covered by our simulation (50 Myr). It is entirely plausible that some cooling would happen at later times (see Gaspari et al. 2012a), but we did not explore this possibility here. Cold gas masses of $1 - 5 \times 10^5$ M$_\odot$ are typical, with periods of much lower or no cold gas found in the galaxy.

As a numerical convergence test we run a model identical to *LM-FB1000* but with a grid resolution of 2 pc. The results are illustrated in the right panels of Figure 8 by the orange lines. While the detailed pattern of the cold gas mass evolution differs, the important result — the generation of an extended, $\sim 10^5$ M$_\odot$ cold ISM phase, even where $t_{cool}/t_{acc} > 10$ — is validated.

6 DUST IN THE HOT AND COLD GAS

6.1 Central Galaxy

As mentioned in the Introduction, the dust content of the cold gas is a crucial test for its origin. The necessary first step is to understand the grain evolution in the hot ISM. This has been investigated in detail by Tsai & Mathews (1995, 1996), Temi et al. (2003), Dwek et al. (1990), Donahue & Voit (1993), Hensley et al. (2014). Stellar ejecta continuosly supply dust to the ISM, at a rate of $\delta_* \dot{M}_* \approx 10^{-3}(M_*/10^{11}$ M$_\odot)$, assuming $\delta_* = 1/150$. In Tsai & Mathews (1995) and Temi et al. (2003) it is argued that stellar ejecta are quickly heated to the hot ISM temperature (see also Mathews 1990) in a timescale $\lesssim 10^6$ yr (a fraction $\lesssim 20\%$ of it may remain cold, according to the calculations by Parriott & Bregman 2008). Dust grains, as they come in contact with $\sim 10^7$ K gas, are sputtered away with a timescale $\tau_{sputt} \sim 0.03/n_p$ Myr (which translates in $\tau_{sputt} \lesssim 10^5$ yr in the galaxy core and $\tau_{sputt} \sim 3 \times 10^6$ yr at $r = 10$ kpc), short enough to make grains be disrupted essentially where they originate.

Our model for the dust evolution in the hot gas agrees with the aforementioned calculations very well. Dust source

---

[8] In these systems hot gas could in principle still cool through the dust assisted cooling process described in Mathews & Brighenti (2003b).
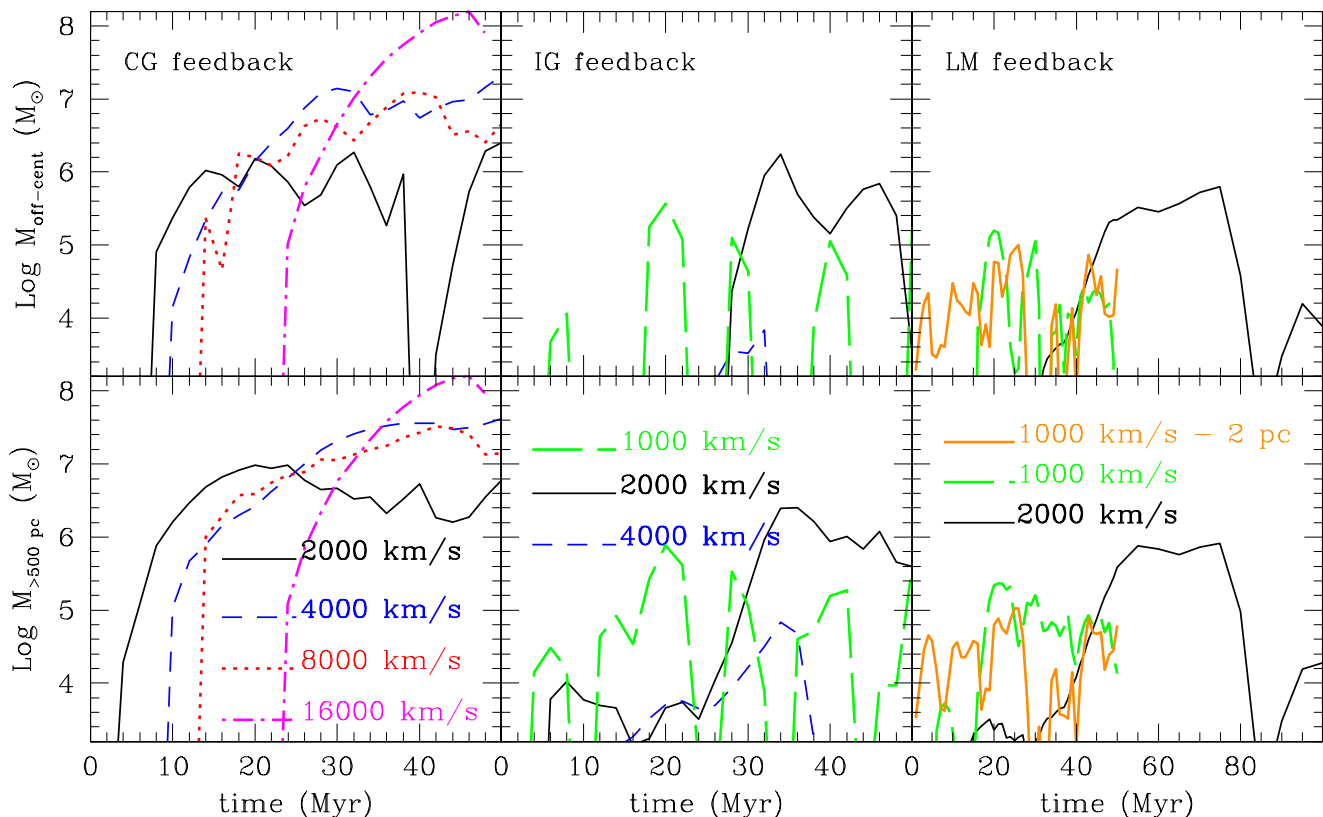
Figure 8. *Upper panel:* time evolution of the cold gas mass in the off-center region ($R > 150$ pc, $z > 500$ pc) for feedback models *CG-FB2000*, *CG-FB4000*, *CG-FB8000*, *CG-FB16000* (left panel), *IG-FB1000*, *IG-FB2000*, *IG-FB4000* (middle panel) and for *LM-FB1000* and *LM-FB2000* (right panel, notice that the time axis extends to 100 Myr in this latter case). *Lower panel:* as above for the total cold gas mass in the off-center region $r > 500$ pc.

and sink terms result, for the *CG* model, in an almost constant ISM dust-to-gas ratio $\delta \sim 3 \times 10^{-6}$. Before the outflow starts the total mass of dust present in the gas in the whole system is $M_{\rm dust} \sim 7.4 \times 10^4$ M$_\odot$, of which only $\sim 5 \times 10^3$ M$_\odot$ reside in the central region within $r_{\rm e} = 10$ kpc. These numbers are very similar to those of the steady state model for interstellar dust in NGC 5044, presented in Temi et al. (2007), where it has been showed that the observed fluxes at 70 μm and 170 μm are a factor $50 - 100$ higher than expected if the only source of cold dust were the stellar winds. The excess dust in NGC 5044 is spatially correlated to the warm ($T \sim 10^4$ K) gas (see also Gastaldello et al. 2009).

Gas cooling out of the hot phase initially shares the aforementioned low dust content. However, dust can grow in cold gas by accretion of condensable elements onto pre-existing grains, as outlined in Section 2. We find that dust accretion is never significant for the cold blobs found in our simualtions. The increase in the dust-to-gas ratio of cold gas is modest, leading to an average $\delta_{\rm cold} \lesssim 10^{-5}$ after 50 Myr, close to the dust-to-gas ratio of the hot phase. We see little variation in the dust-to-cold gas ratio between models. The inefficient dust growth originates from both the relative low density of the cooled gas clouds (usually $\lesssim 50$ cm^{-3}) and their short lifetime. Off-center cold blobs, in fact, are young objects, with life span $\sim t_{\rm dyn} \lesssim 10^7$ yr, after which they

settle in the galaxy core or in the cold filament along the $z-$axis[9].

Therefore, a robust prediction of our calculations is that internally produced, spatially extended cold gas is very dust-poor. Evidently, any spatially extended (and therefore recently formed) dusty cold gas in isolated elliptical galaxies must have a different origin, as for example cooling of dusty stellar ejecta mixed with local hot gas (Mathews & Brighenti 2003b; Temi et al. 2007) or accretion of external gas (e.g. Davis et al. 2011). On the contrary, cold gas can reside in the $z-$axis filament long enough, and with density large enough, to allow dust accretion be effective. At the end of the feedback simulations, at $t = 50$ Myr, the dust-to-gas ratio in the filament reaches values of $\sim 5 \times 10^{-3}$. For the same reason, dust growth can also be an important process in old cold gas located at the very center of a large fraction of ellipticals, known to be dusty (e.g. Tran et al. 2001; Martel et al. 2004; Lauer et al. 2005; Simões Lopes et al. 2007; Alatalo et al. 2013).

We remark that the low dust content for the cooled hot gas might also lead to a low H_2 and CO content (with respect to the Galactic standards), even if the temperature dropped

---

[9] We neglect here the potential role of hot gas rotation, which would generate a large disk of cold gas, several kpc in radius (e.g. Brighenti & Mathews 1997a).
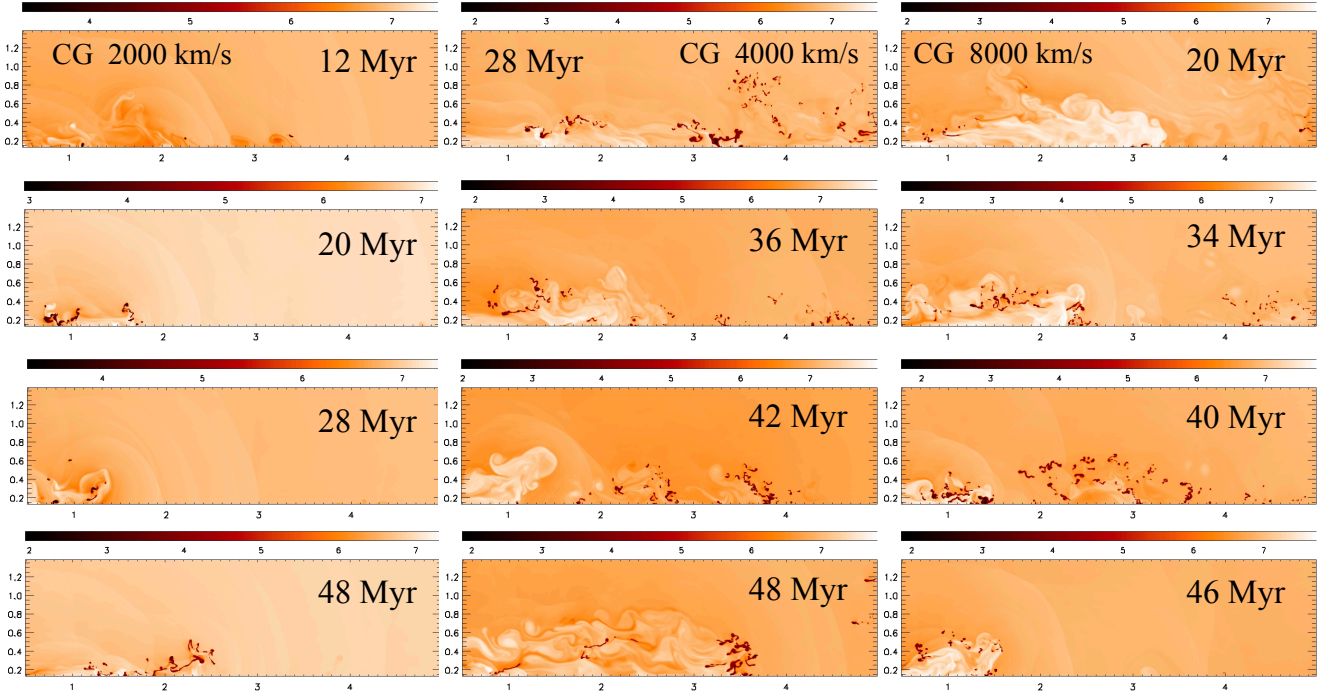
Figure 9. *Left column:* temperature maps for model *CG-FB2000* at four different times: $t = 12, 20, 28, 48$ Myr, from top to bottom. The z-axis is horizontal, the R-axis is vertical. Units are kpc. Time is measured since the switch on of the AGN outflow (which lasts 2 Myr). *Central column:* temperature maps for model *CG-FB4000*, shown at 28, 36, 42 and 48 Myr. *Right column:* temperature maps for model *CG-FB8000* at $t = 20, 34, 40$ and 46 Myr. Notice that the color scale differs for every panel.
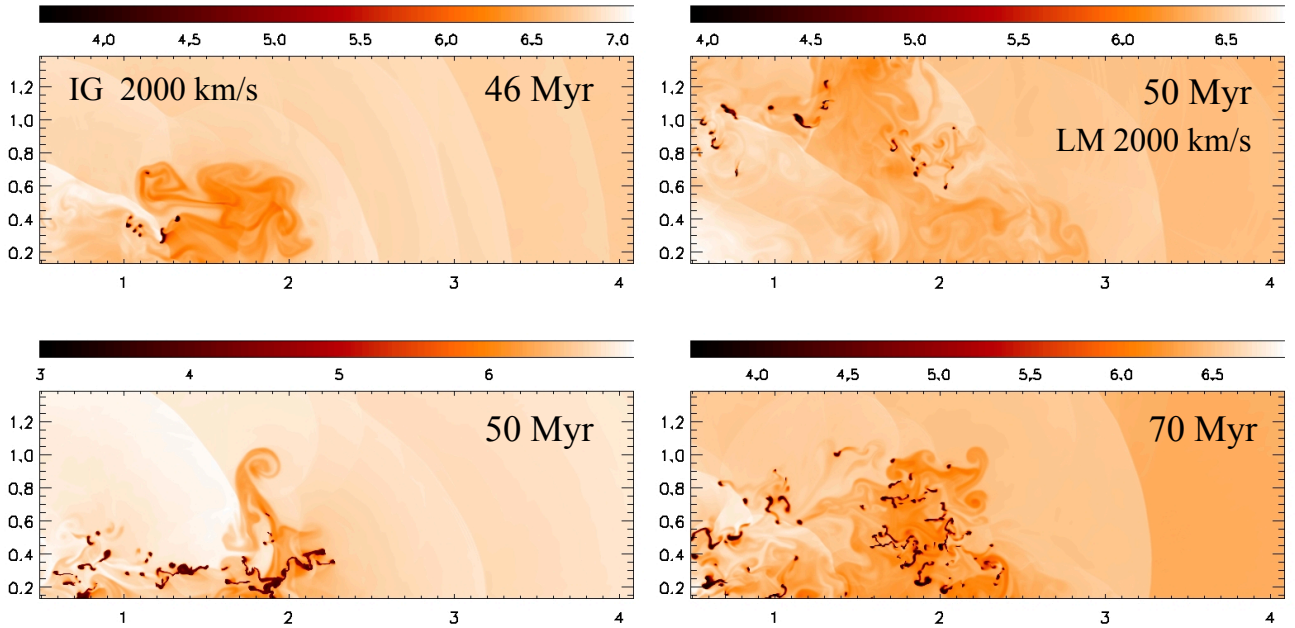
Figure 10. *Left column:* temperature maps for *IG-FB2000* model of the isolated elliptical. The z-axis is horizontal, the R-axis is vertical. Units are kpc. *Right column:* same for *LM-FB2000* model. Notice that the color scale differs for every panel.

to very low values $T \lesssim 100$ K (see Cazaux & Spaans 2009). Furthermore, dustless cold gas would not be effective in absorbing stellar radiation and would be hardly detectable in dust extinction maps. Some indication of dust-poor molecular gas in NGC 5044 is provided by the ALMA observation presented in David et al. (2014). Mainy molecular associations have been found the inner ~ 2.5 kpc, for a total molecular mass $\gtrsim 5 \times 10^7$ M$_\odot$. The absorption map presented in David et al. (2014) shows dusty patches that do not correlate with the molecular structures. If the dust poor cooled gas is able to form H_2 and CO in $\lesssim 10^7$ yr, molecular clouds in ETGs would not provide much absorption or extinction, just like observed.

Only the cold $z-$axis filament is expected to have a sizeable amount of dust but, although the formation of this feature is entirely reasonable, we are chary to study in detail its dust properties here, for the reasons explained above.

6.2   Isolated Galaxy

The hot gas dust content in the standard CF model for the IG is 2.7×10^6 M$_\odot$. This amount is more sizeable than in the corresponding *CG* model because of the lower average ISM density, which makes the grain sputtering process less efficient ($\tau_{\rm sputt} \propto n^{-1}$), especially in the outer galactic regions. Within $r = 10$ kpc $M_{\rm dust,hot} = 1.4 \times 10^5$ M$_\odot$, while within $r_{\rm e} = 6$ kpc we have $M_{\rm dust,hot} = 3.6 \times 10^4$ M$_\odot$. The dust-to-gas ratio in the hot ISM is now larger than that of the *CG*, rising from $\delta_{\rm hot} \sim 10^{-5}$ in the very center, to $\delta \sim 10^{-3}$ at the effective radius (6 kpc).

The higher $\delta_{\rm hot}$ leads to a higher average dust-to-gas ratio for the off-center cold ISM phase, $\delta_{\rm cold} = 3-10 \times 10^{-5}$, for both the single outflow and the feedback models. Higher velocity outflows typically generate higher $\delta_{\rm cold}$ because gas cools at larger radii, where $\delta_{\rm hot}$ is also larger. The situation is therefore similar to that depicted for the *CG* model: spatially extended cold gas originated by cooling of the hot phase is predicted to exist in real ellipticals with AGN feedback. However, it is expected to be almost dustless; any dust-rich cloud or filament has likely been accreted or ejected from the nuclear region, where dusty cold gas is known to be present.

In the $z-$axis filament, the dust-to-gas ratio never exceeds 8×10^{-5}. The lower value with respect to the *CG* model is mostly due to the lower density in the *IG* filament, which makes the grain growth process relatively inefficient.

6.3   Low Mass Galaxy

The *LM* galaxy has the lowest average hot ISM density among our models. This makes the sputtering time longer and the dust content more substantial than in the *CG* and *IG* systems, with an average dust-to-gas ratio 3.8×10^{-3} within 10 kpc and 1.4×10^{-3} within $r_{\rm e}$, at the time of the AGN activation. The dust mass in the hot gas is $M_{\rm dust,hot} = 1.7 \times 10^4$ (or 1.3×10^5) M$_\odot$ for $r \leqslant 3.16$ (or 10) kpc, respectively. The cold clumps and filament generated by the AGN outbursts are both characterized by average $\delta_{\rm blob,fil} \sim 10^{-4} - 10^{-3}$, with the largest values found for model *LM-FB2000*.
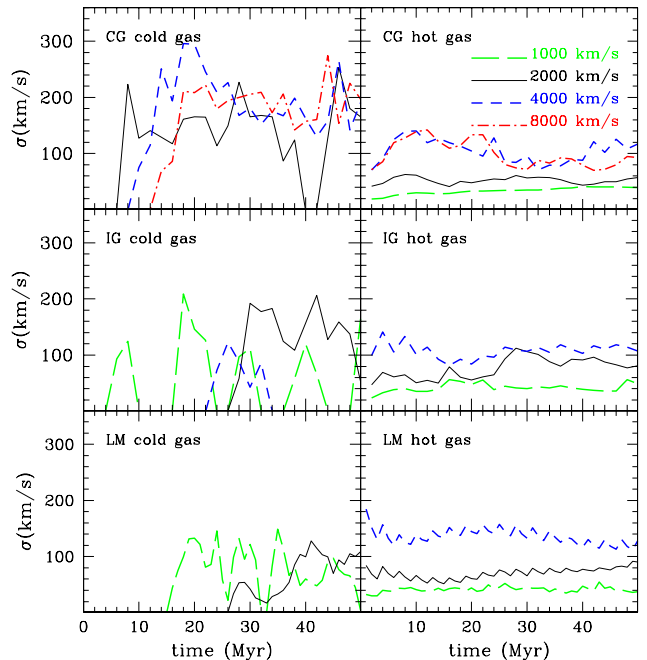
Figure 11. *Left panels:* time evolution of cold gas velocity dispersion for gas in the off-center region defined by $0.5 < z < 5$ kpc, $0.15 < R < 3$ kpc. The *CG-FB*, *IG-FB* and *LM-FB* models are displayed in the top, middle and bottom panels, respectively. For each system we show the feedback model with $v_{\rm jet} = 1000, 2000, 4000$ km s^{-1} with long-dashed green, solid black and dashed blue lines (for the CG model we also show the $v_{\rm jet} = 8000$ km s^{-1} model with a dot-dashed red line), respectively. *Rigt panels:* same for the hot gas.

7   GAS VELOCITY DISPERSION AND COLD INFLOW/OUTFLOW

7.1   Central Galaxy

It is interesting to investigate the gas velocity dispersion generated by the AGN outflow. The chaotic motion triggered by the outflow expansion and the following buoyant motion of low-density regions cause the density perturbations leading to widespread cooling. Also, it promotes the circulation of the metals injected by the SNIa occurring in the galaxy (e.g. Rebusco et al. 2006; Gaspari et al. 2011a,b, 2012a). Recent X-ray observations provide estimates on the turbulent velocity in clusters and groups, albeit with large uncertainties (Werner et al. 2009; Sanders et al. 2011; de Plaa et al. 2012). For NGC 5044 and NGC 5813 the latter authors find $320 < v_{\rm turb} < 720$ km s^{-1} and $140 < v_{\rm turb} < 540$ km s^{-1} respectively, measured in the central ~ 10 kpc region.

In the pure cooling flow model, before the onset of the AGN feedback, the hot gas 3D, mass-weighted velocity dispersion is extremely low, $\sigma_{\rm hot} \sim 14$ km s^{-1} (here and in the following, the velocity dispersion is measured in the region $0.5 < z < 5$ kpc, $0.15 < R < 3$ kpc, corresponding to the off-center region where the numerical resolution is higher)[10].

---

[10] We estimate the mass-averaged velocity dispersion as $\sigma^2 = \sigma_z^2 + 2\sigma_R^2$, where the $z-$component is $\sigma_z^2 = \int (v_z - \hat{v_z})^2 \rho dV / \int \rho dV$ and the integrals are calculated on the

This value for $\sigma_{\rm hot}$ essentially reflects the (smooth) radial velocity gradient typical for cooling flows in the region considered. The single outflow event increases the hot gas turbulence, with typical velocities $\sigma_{\rm hot} \sim 15, 35, 60, 100$ km s^{-1} for *CG1000, CG2000, CG4000* and *CG8000* respectively, measured few Myr after the AGN outburst. This chaotic motion slowly decays, reaching values $\sigma_{\rm hot} \sim 15, 30, 30, 40$ km s^{-1} at $t = 50$ Myr. The cold gas, when present, usually shows larger velocities, with typical values $\sigma_{\rm cold} \sim 80-150$ km s^{-1}, essentially independent on the outflow velocity. These numbers compare well with observed cold gas velocity dispersion in massive ellipticals (Caon et al. 2000; Werner et al. 2013).

In Figure 11 we show the velocity dispersion for the cold and hot ISM for the feedback models. Again, $\sigma_{\rm hot}$ generally increases with $v_{\rm jet}$ (although models *CG-FB4000* and *CG-FB8000* are almost undistinguishable). Typical $\sigma_{\rm hot}$ values range between 50 and 100 km s^{-1}. The obvious difference with respect to the single outflow models is that $\sigma_{\rm hot}$ stays approximately constant in time, as expected for a self-regulating feedback scenario.

We also find that $\sigma_{\rm hot}$ is strongly dependent on the position. As expected, the turbulence is much stronger near the jet axis. If we measure $\sigma_{\rm hot}$ in the sector $R \geqslant z$ (that is, far from the jet axis) we get values a factor $1.5 - 2$ lower than in the sector $R \leqslant z$. This implies that any mixing and turbulent heating should be much less effective in the region near the plane of symmetry $z = 0$.

The values for $\sigma_{\rm hot}$ we find are significantly lower than those observed. Although estimates for $\sigma_{\rm hot}$ in real galaxies are still sparse, this discrepancy may indicate that AGN feedback is more powerful than the one considered in the present paper (see, e.g. Gaspari et al. 2012a). Stronger outbursts are indeed needed to prevent the excessive total cooling rate observed in our simulations. A further possibility to explain the observed large turbulent velocity is the effect of merging and accretion into the system. For instance, in NGC 5044 a pair of cold fronts are visible within the inner ~ 70 kpc region, likely generated by the accretion of a galaxy or a small group (Gastaldello et al. 2009; David et al. 2009). The large (~ 150 km s^{-1}) peculiar velocity of the central galaxy with respect to the mean group velocity supports this scenario.

Also for the feedback models we find that $\sigma_{\rm cold} \gtrsim \sigma_{\rm hot}$. This is in part explained by the tendency of the gas to cool in regions of localized stronger turbulence. In addition, once cooled to low temperatures, the blobs decouple dynamically from the hot gas (although their motion is never totally ballistic[11]), and this results in a further increase of $\sigma_{\rm cold}$. Overall, the recently formed cold gas moves in a somewhat chaotic way, with velocities similar to those found by Caon et al. (2000). We note here that in our simulations no cold gas is dragged to large radii from the central region. This indeed must be expected, given the high density and small cross section of the cold clouds, which make them almost immune to drag by hot gas or entrainment. In models with

volume defined in the text. The $R-$component is computed in a similar way.

[11] The fact that single blobs are not properly resolved in our simulations and the effect of numerical viscosity may play a role in maintaining a slight coupling between hot and cold gas. We did not investigate this in detail.
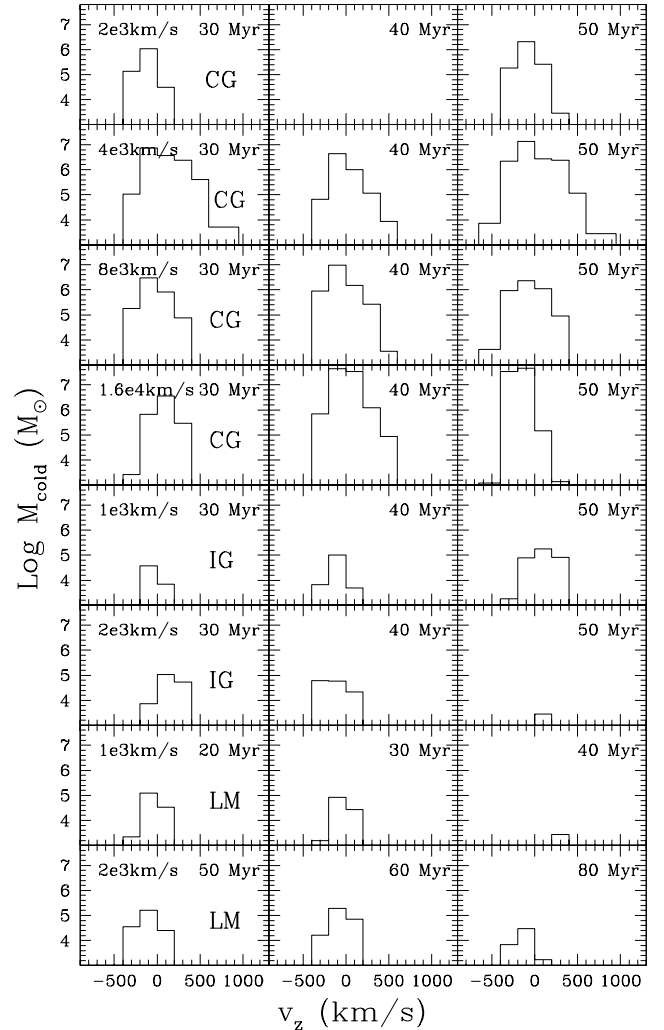
Figure 12. Distribution of the cold gas in the z-axis velocity space for various feedback models at several times. Positive velocity indicate outflowing gas. Every row represents a model, indicated on the left panel of each row (for example in the top row is shown the *CG-FB2000* run).

large $v_{\rm jet}$ we do see cold blobs moving outward together with the hot gas, but this is because the cold gas forms from the outflowing hot gas and initially shares the same motion.

At any time cold gas clouds with both positive (outflowing) or negative (inflowing) radial velocity are present. Often gas cools and condenses out from outflowing hot gas, resulting in a cold outflow. We note that molecular outflows are now commonly detected in AGN hosts (e.g. Cicone et al. 2014; Tadhunter et al. 2014), albeit in systems different than the group centered massive elliptical simulated here. In our scenario (see also Li & Bryan 2014; Sharma et al. 2012) the cold gas is not directly accelerated by the AGN, but merely forms in the already forward moving hot gas[12]. As for the mass and spatial disposition, the distribution of the off-center ($0.5 < z < 5$ kpc, $0.15 < R < 3$ kpc) cold gas mass

[12] In a very recent paper Costa et al. (2014) have shown that hot gas cooling can generate cold outflows in QSO hosts.

in the velocity space, shown in Figure 12 for several models, also varies in an unpredictable way. For most models/times there is a slight tendency for the cold gas to prefer outward motion, but the effect is subtle. Typical velocities of $\sim$ few km s^{-1}, both positive and negative, along the outflow symmetry axis are always present. It is interesting that the cold gas velocity distribution does not depend in an obvious way on the outflow velocity v_{jet} — the model *CG-FB16000* does not show a high velocity tail as might be expected.

7.2 Isolated and Low Mass Galaxies

For these models, the hot gas velocity dispersion before the AGN onset is $\sigma_{\mathrm{hot}} \sim 5$ km s^{-1}, somewhat less than in the *CG* case.

The single AGN outflow in the *IG* generates chaotic motion with $\sigma_{\mathrm{hot}} \sim$ 40, 80, 120, 200 km s^{-1} for *IG1000, IG2000, IG4000* and *IG8000* (few Myr after the feedback episode, again measured in the region $z < 5$ kpc, $R < 3$ kpc). The ISM motion dissipates to reach $\sigma_{\mathrm{hot}} \sim 20$ km s^{-1} at $t = 50$ Myr for *IG1000* and *IG2000*, and $\sigma_{\mathrm{hot}} \sim 60$ km s^{-1} for *IG4000* and *IG8000*. As for the *CG* model, *IG* also shows a large velocity dispersion for the off-center cold gas (run *IG2000*), with $\sigma_{\mathrm{cold}} \sim 100$ km s^{-1}. Again, the main reason for this discrepancy is the different spatial regions probed by the the two gas phases. While for the hot gas the whole off-center volume is used to compute σ_{turb}, the cold gas is present only in the smaller region $(R, z) \lesssim (0.8, 2.5)$ kpc, where indeed the hot gas turbulence is stronger and comparable to that of the cold gas (~ 100 km s^{-1}).

The *IG* feedback simulations exhibit similar charchteristics for the AGN-induced random motion as for the *CG-FB* models (Figure 11). The hot phase 3D velocity dispersion varies from ~ 50 to ~ 100 km s^{-1}, while the cold gas shows values about twice as those of the hot gas.

For the low mass galaxy *LM*, the chaotic ISM motion resulting from the AGN activity is similar to that of the *IG-FB* models, and the 3D gas dispersion velocity is shown in the bottom row of Figure 11. We note that for the off-center cold gas of these *LM-FB* models σ_{cold} is somewhat lower with respect to the *CG-FB* and *IG-FB* runs, a consequence of the lower free fall velocity of the *LM* galaxy.

For these isolated galaxies the velocity distribution of the cold gas (Figure 12) is narrower than for the *CG* model. For most of the time cold outflows are limited to ≈ 200 km s^{-1}, while the inflowing portion of the cold ISM commonly reaches ~ 400 km s^{-1}.

8 ENERGETICS

In this work we decided to be conservative regarding the strength of the AGN feedback considered. We deliberately chose to adopt low power outflows because they are expected to be the most common in normal elliptical galaxies. For instance, even in the spectacular archetype of AGN-ISM interaction NGC 5044, the power associated to the cavity system is only $\lesssim 6 \times 10^{42}$ erg s^{-1} (David et al. 2009). More typical

cavity powers for massive ellipticals or groups range from 10^{41} to 10^{42} erg s^{-1} (Panagoulia et al. 2014)[13].

We do not show here the detailed evolution of the outflow energetics, but limit ourself to a discussion of the basic properties of our feedback simulations (see Gaspari et al. 2012a, for a detailed analysis of more sophisticated models). In agreement with the forementioned paper we find that the total energy injected by the AGN slightly increases with v_{jet} (although this trend reverts for *CG-FB8000*). For models *CG-FB1000, CG-FB2000, CG-FB4000, CG-FB8000* and *CG-FB16000* the total outflow energy $E_{\mathrm{jet}}^{\mathrm{tot}}$ delivered to the ISM at $t = 50$ Myr is 2.5×10^{55}, 7.0×10^{55}, 1.8×10^{56}, 7.2×10^{55} and 6.0×10^{56} erg, respectively. As found in Gaspari et al. (2012a) we also note a definite trend for the duty cycle (defined as the ratio between the time in which the outflow is active to the total time of the simulation) to decrease with increasing v_{jet}: 2.3×10^{-2}, 7.1×10^{-3}, 1.9×10^{-3}, 1.5×10^{-3} and 6.7×10^{-5} for the models listed above. This is a signature of a self-regulating mechanism. In model *CG-FB16000* only a dozen AGN outbursts occur. The average outflow power, $P_{\mathrm{jet}} = E_{\mathrm{jet}}^{\mathrm{tot}}/(50$ Myr $\times$ duty cycle) is 6.9×10^{41}, 6.2×10^{42}, 6.0×10^{43}, 3.0×10^{43} and 6.7×10^{45} erg s^{-1} for the five considered models. Single AGN outbursts show a typical power variation of ~ 5 with respect to the mean value. Model *CG-FB16000* clearly shows a different feedback regime with respect to the lower v_{jet} calculations. The AGN heating operates through a sequence of relatively infrequent, very powerful outbursts, separated by quescence periods lasting several Myr. While this model is successful in reducing the total cooling rate down to acceptable values, the central ISM often shows temperatures $\gtrsim 2$ keV, higher by a factor of ~ 2 than those in the center of real galaxies/groups. The difficulty for the AGN heating to simultaneously halt gas cooling and preserving low central temperatures is well known and will not be discussed here (see, e.g. Brighenti & Mathews 2002; Gaspari et al. 2012a).

For the isolated galaxy *IG* the outflows energetics is somewhat different with respect of that of the *CG* models. For instance, the total energy injected in the ISM is now 5.4×10^{55}, 1.1×10^{56} erg for model *IG-FB1000* and *IG-FB2000*, while the duty cycle is 3.3×10^{-3}, 8.1×10^{-4} and 5.9×10^{-5} for *IG-FB1000, IG-FB2000* and *IG-FB4000*.

9 DISCUSSION

9.1 The Cold ISM of Elliptical galaxies

Despite of the accuracy of the simulations presented here, we are well aware that many results are subject to quantitative uncertainties. The physics of the AGN feedback process still eludes our understanding and has been represented only schematically. A source of error which is difficult to evaluate in the simulation outcomes originates from the sometimes neglected numerical overcooling, together with the intrinsic complexity of the cold-hot gas interaction (which is impossible to reproduce in current galaxy-wide calculations).

---

[13] It should be noted here that these estimates for low mass systems might be inaccurate, if very deep Chandra observations are not available. Furthermore, the fraction of outflow power dissipated in shocks is poorly known.

Notwithstanding this cautionary note, we believe that a solid result of our study (see also Brighenti, Mathews and Temi, 2015) is that AGN activity triggers spatially extended gas cooling from the hot ISM phase. This happens for a wide range of outflows parameters, a fact which makes this prediction robust despite the uncertainties in the AGN feedback process[14]. Of course, the net effect of the energy injected by the AGN is to reduce (or suppress) the total cooling rate (e.g. Gaspari et al. 2012a).

The off-center cold gas has an erratic distribution, following the cycle of the AGN feedback, activated (by design) by the random presence of cold (dropped-out) gas near the black hole (Pizzolato & Soker 2005, 2010; Gaspari et al. 2013, 2014). The exact amount of cold gas depends on the outflows parameters (velocity, especially) and is therefore somewhat uncertain. In our *CG* model (tailored on NGC 5044) we find that $\sim 10^5 - 10^8$ M$_\odot$ of off-center cold gas are typically present, depending on the feedback parameters. For the isolated galaxies *IG* and *LM* the amount of the cold gas is reduced, but still significant: $\sim 10^4 - 10^6$ M$_\odot$. These values compare well with observations (Macchetto et al. 1996; Caon et al. 2000; David et al. 2014). Especially for the isolated systems, there are times when the cold gas is absent or negligible (see Figure 8). Indeed, that the mass budget of the cold ISM phase undergoes unpredictable variations (cfr. Figure 8), again in pace with the AGN activity. It seems therefore plausible that AGN-induced cooling can explain, at least in part, the large fraction of intermediate/massive ellipticals with detectable Hα emission or even molecular gas, if H_2 and CO can form fast enough in the dust-poor cooled gas.

Our simulations cannot follow the evolution of the cooled gas with the accuracy necessary to calculate what fraction of it ends up in molecular form. H_2 can form by both grain surface and gas phase reactions, with the dust grain processes dominant for gas metallicity larger than $Z = 10^{-4} - 10^{-5}$ solar (e.g. Cazaux & Spaans 2009, and references therein). The cold gas in our simulations has $\sim$ solar metallicity, but the dust-to-gas ratio is $\delta \sim 10^{-5}$. This latter value is similar to the dust-to-gas ratio of the model with metallicity $Z = 10^{-3}$ solar in Cazaux & Spaans (2009), which we can therefore adopt to make order-of-magnitude considerations. Using the H_2 formation rates given in their Fig. 6, we find that the typical H_2 formation timescale is ≈ 1 (50, 2000) Myr for gas density $\sim 10^3$ (10^2, 10) cm^{-3}. Unfortunately, for the highest quoted densities, these numbers are close to the lifetime of our simulated cold clouds, therefore no strong conclusions can be drawn about the presence of molecular gas in the blobs. For $n = 10$ cm^{-3} no H_2 is expected to form. It is unclear which density the gas cooled to $T \lesssim 100$ K would reach — our simulations do not have the resolution to properly resolve the structure of the cold clouds. Moreover it seems likely that magnetic or turbulent support would be important in regulating the density profiles of the clouds. Thus, in order to properly investigate this topic, a better calculation for the thermal and dynamical evolution for the clouds is needed, coupled with a H_2 (and

CO) formation model which takes into account the chemical properties of the cooled ISM and the appropriate dissociating UV field. This is beyond the scope of the present paper, although such a calculation would be crucial to properly interpret the molecular associations detected in the central galaxy NGC 5044 by David et al. (2014).

Davis et al. (2011) found that most galaxies show kinematically misaligned cold gas. This is usually interpreted as evidence that gas has been accreted, through (minor or major) merging or from smooth cosmological accretion. That is, that cold gas has an external origin. Another possibility is the scenario proposed by Lagos et al. (2014), where misaligned cold gas is generated internally by cooling of a twisted hot gas halo. Undoubtedly these processes occur and may well explain the bulk of the misaligned cases. However, it is interesting to note that AGN cooling also predicts kinematically decoupled cold gas-stellar systems. In fact, cold gas forms and moves preferentially along the outflow axis, which may well be the rotation axis of the stellar body of the galaxy. Therefore, looking to the system from a generic viewing angle, stars and cold gas would indeed show a kinematic misalignment, even though the gas origin is internal. Of course, the cold gas in this simple scenario would likely show irregular appearance and kinematics — smoothly rotating misaligned gas can be internally generated only through the model described in Lagos et al. (2014).

Thus, AGN can play a double role in the galaxy life. It strongly decreases the gas cooling process, solving the cooling flow problem and quenching the star formation, causing the migration of the galaxy to the red sequence. However, the dynamical interaction with AGN outflows keeps the ISM "alive", giving rise to the episodic presence of a significant cold phase and possibly triggering sporadic, weak star formation events which could explain in part the recent SF activity commonly detected in ETGs (Trager et al. 2000; Kaviraj et al. 2007). While minor mergers are an attractive explanation (Kaviraj et al. 2009), we point out that AGN-induced hot gas cooling is a natural, internal process which also potentially leads to low-level SF.

9.2 $H\alpha$ emission from warm clouds

Cold blobs, although they share similar properties, are made up of gas which has cooled down to different temperatures ($1.8 \lesssim log\, T_{\rm blob} \lesssim 4$). Here we provide a rough estimate of the expected $H\alpha$ luminosity of the spatially extended cold gas, which in turn depends on the amount of the ionized cold ISM. Column density of blobs, calculated as $N = \langle n \rangle l$, where $\langle n \rangle$ is an average of the blob number density and l is its linear size, spans the range $3 \times 10^{19} \lesssim N \lesssim 3 \times 10^{21}$ cm^{-2}. Their number density is in the range $0.4 \lesssim n \lesssim 50$ cm^{-3} and their (smallest) characteristic size is usually no more than few tens of parsec. This column density is usually larger than the maximum column density $N_{\rm ion}$ that can be photoionized by the local ionizing photon field, which includes the contributions of both the stellar radiation (usually the dominant one at the clouds location) and the intergalactic background.

The mass fraction M_{ion} of ionized gas in blobs has been estimated in order to derive the actual contribution of cooled gas emitting in $H\alpha$ band. Assuming that blobs are spherical, the problem for a single blob reduces to an inverse Strömgren

---

[14] Numerical experiments with different feedback methods, such as jets and cavities generated by cosmic rays (Perrotta et al., in preparation), yield qualitatively similar results.

sphere: $4\pi R_s^2 \Delta R n^2 \alpha = 4\pi R_s^2 n_\gamma c$, where R_s is the radius of the blob (or the smallest size of an elongated clump), ΔR is the thickness of the actually ionized shell, n and n_γ the density of the gas inside the cool clump and the local ionizing photon density respectively, c the speed of light. Here, the number of recombinations expected in the spherical shell has been equated to the number of ambient incident photons which photoionize the outer layer of the blob; the recombination coefficient is $\alpha \simeq 4 \times 10^{-13}$ cm^3 s^{-1} (Spitzer 1978). The ionizing photon density $n_\gamma(r)$ has been estimated by following Brighenti & Mathews (1997b), who considered an elliptical galaxy of stellar mass 7.5×10^{10} M$_\odot$ and effective radius 1.72 kpc, by scaling their $n_\gamma(r)$ for the different stellar masses and effective radii of our galaxies. The resulting ionizing photon density profile writes $n_\gamma = A\, r_{\rm kpc}^{-1.5}$ cm^{-3}, where the constant $A = 10^{-3}, 3 \times 10^{-3}, 2.4 \times 10^{-3}$ for CG, IG and LM respectively.

Solving for ΔR, the thickness of the actually ionized layer of a typical blob which is located at a certain distance from the center at a given time and which has a certain density is estimated. From the value of $\Delta R \approx (20, 70, 58)\, r_{\rm kpc}^{-1.5}/n^2$ pc (for models CG, IG, LM) it is possible to calculate the ionized mass of the blob:

$$M_{ion} \sim 4\pi R_s^2\, \Delta R\, \rho_{blob} \sim 3 M_{blob} \frac{\Delta R}{R_s}\ , \qquad (6)$$

where ρ_{blob} is the density corresponding to the aforementioned n and $R_s \simeq 30$ pc. Unfortunately, we find that the fraction of ionized gas in a single clump varies widely, depending on its density and location in the galaxy, spanning the range $0.2\% \, M_{blob} \leqslant M_{ion} \leqslant 50\% \, M_{blob}$.

It is difficult and likely not worthy, given the uncertainties, to calculate the percentage of ionized mass of every single blob. However, density and temperature of a large number of examined clumps span the aforementioned ranges; the simulation time does not play a crucial role in determining the density or the temperature of appearing (just cooled) blobs; on the contrary, the evolution of blobs, when it can be followed, shows that old blobs are denser than short-lived ones and that they are often the result of the merging of ligther clumps.

A further difficulty is that the simulated blobs are under-pressurized with respect to the ambient gas, sometimes by a factor of $10 - 100$ (see also Li & Bryan 2014). If temperatures of blobs are thought to be reliable, the expected pressure equilibrium would produce a corresponding increase in the density (neglecting magnetic support)[15]. This, in turn, leads to a smaller linear size of the blob. The combined effect of the increase of ρ_{blob} and the drop in l lowers the mass fraction of ionized gas by a factor $\sim 5 \times 10^{-4}$ when a typical blob of given mass is thought to have a two order of magnitude larger density. The aforementioned increase in ρ_{blob} would lead to the enhancement of dust growth in blobs, too, since $\dot{\rho}_{\,growth} \propto \rho$ (see section 2). However, a cloud is expected to reach pressure equilibrium after a sound crossing time τ_{sc}; τ_{sc} spans the range $2 - 20$ Myr when blobs of a typical size of 30 pc and of different temperatures are

considered. The long τ_{sc} might be the responsible for the lack of pressure equilibrium in coldest blobs, most blobs being younger than their τ_{sc} and more short living. Observations indicate low thermal pressure in the ionized gas. For instance, in the central regions of M 87 the [S II]λ6716/6731 line ratio reveals electronic number densities ($n_e \simeq 25$ cm^{-3}) in the emission line gas (Werner et al. 2013) which are lower than the ones obtained if pressure equilibrium is supposed ($n_e \simeq 100$ cm^{-3} in gas with $T \sim 10^4$ K if a typical number density of $n_{e,\,hot} \simeq 0.1$ cm^{-3} in the $T_{hot} \sim 10^7$ K surrounding medium is adopted).

These considerations suggest to not attempt a rigorous calculation of the $H\alpha$ luminosity in our simulated galaxies. Nevertheless we are able to give interesting upper limits in $L_{H\alpha}$ generated by the warm non-nuclear gas. We rerun several models similar to those described in the previous sections, but this time setting $T = 10^4$ K as lower limit in the gas temperature and assuming that all the cold gas is ionized. In this way we can calculate firm upper limits for $L_{H\alpha}$. For the CG-FB system we find for the off-center gas an average value $L_{H\alpha,blob} \approx 5 \times 10^{39}$ erg s^{-1}, with typical variations of ~ 5 among the various CG models. The z-axis filament can be much brighter, $L_{H\alpha,fil} \approx 10^{40} - 10^{42}$ erg s^{-1}, but most of its gas is indeed expected to be neutral or molecular. The off-center warm gas in IG and LM models is fainter than for the CG, an obvious result of the less substantial cold ISM phase in these systems. The upper limits for the IG-FB (when off-center cold gas is present — see Figure 8) vary in the range $L_{H\alpha,blob} \approx 10^{37} - 10^{39}$ erg s^{-1}, while LM-FB never exceeds $\sim 5 \times 10^{37}$ erg s^{-1}. As before, the upper limits for the filament can be one or two order of magnitude brighter that those for off-center blobs.

10　CONCLUSIONS

In this paper we have presented hydrodynamical models of AGN outflows expanding in the hot ISM of elliptical galaxies. We have designed these numerical experiments to test the idea that AGN feedback, while strongly quenching the total cooling rate, can nevertheless stimulate some degree of hot gas cooling at a few kpc distance from the galaxy center (see also Brighenti & Mathews 2002; Gaspari et al. 2012a,b; Sharma et al. 2012; McCourt et al. 2012; Costa et al. 2014). This process can generate a persistent cold ISM phase in early-type galaxies. We explore the feasibility of this scenario in galaxies of different mass and hot gas content, ranging from X-ray bright, group centered ellipticals to galaxies of intermediate mass with a relatively thin hot gas halo.

We have deliberately chosen a simple AGN feedback scheme. We assume that AGN injects energy and momentum through non relativistic outflows, activated by the gas cooling in the inner 100 pc (see e.g. Gaspari et al. 2012a). We focus here on relatively weak feedback, likely the most common regime in normal galaxies. The most significant results of our investigation can be summarized as follow:

i) The interaction between AGN outflows and the ISM generates non-linear density perturbations in regions of converging flows. These perturbations trigger localized hot gas cooling at distances of several kpc from the galaxy center. This confirms the early results of Brighenti & Mathews (2002) for the CG model and extend them to elliptical galax-

---

[15] Self-gravity, whose effect is not included in the code, cannot physically play a crucial role in attempting to compress blobs and enhance their density, the smaller size of a typical blob being usually far shorter than its Jeans length.

ies of lower mass (*IG* and *LM* runs). Li & Bryan (2014) have shown that this process occurs also in BCGs at the center of massive clusters.

ii) The cooling process and the amount of off-center cooled gas are not sensitive on the parameters of the outflows. This is a key result, given the uncertainties of the AGN feedback mechanism and makes our findings quite robust: AGN outbursts seem to stimulate large distance cooling no matter what.

iii) Off-center cooling occurs when $t_{cool}/t_{ff} \lesssim 70$ (in the unperturbed ISM), but we do not expect that this is a strict threshold. Instead, the spatially extended cooling process, no more closely related to thermal instability when the inhomogeneities are strongly non-linear, depends on the local (perturbation) value of t_{cool}/t_{ff}, that is on the perturbation density contrast (see also Joung et al. 2012). Our calculations suggest that even moderate AGN feedback is sufficient to generate density (entropy) inhomogeneities which cool locally.

iv) The amount and the spatial distribution of the off-center cold ISM is erratic (see Figure 8). For group-centered galaxies (model *CG*), the extended cold phase has a typical mass of $10^6 - 10^7$ M$_\odot$, with time variation of a factor of ~ 5. For isolated galaxies (*IG* and *LM*) periods of no off-center cold gas give turns to episodes of significant cold and extended ISM presence, with mass $\sim 10^4 - 10^6$ M$_\odot$. A possible spin-off result concerns hot gas halos in massive spiral galaxies. Given the similarity between detected hot coronae around disk galaxies and the hot ISM in our LM model, it appears conceivable that any outburst from the central black hole (perhaps similar to the one responsible for the Fermi bubble) could indeed trigger cooling of the hot corona, forming cold clouds which will accrete on the galactic disk.

v) The cold gas initially shares the same kinematics of the hot out of which it forms. Dispersion velocities in the range $150 - 250$ km s^{-1} for model *CG*, $100 - 200$ km s^{-1} for *IG*, $50 - 100$ km s^{-1} for *LM* are typical. This compares well with measurements for the emission line component in ETGs (e.g. Caon et al. 2000), while is generally lower than the values given in Werner et al. (2014) for [CII] emitting gas in a sample of massive ellipticals.

vi) Some gas condenses out from outflowing hot gas, resulting in a cold outflow moving with characteristic velocity of a few 100s km s^{-1} (see also Costa et al. 2014). We also notice that cold gas moving mainly close and along the outflow axis can appear kinematically misaligned with respect to the stars.

vii) We follow the evolution of the dust in both the hot and cold gas. Dust is injected in the hot phase by the stellar mass loss, it is destroyed by thermal sputtering and can grow in the cold clouds by accretion of condensable elements. We find that the off-center cold gas always has a very low dust-to-gas ratio, of the order of $\delta_{cold} \sim 10^{-5}$ for the *GC* and $\delta_{cold} \sim 10^{-3} - 10^{-4}$ for the lower mass systems. Therefore, a strong dust deficiency is the distinctive sign for cold gas originated internally from hot halo cooling. However, we acknolewdge some degree of uncertainty for the latter conclusion. If cold gas densities were grossly underestimated in our simulations (see Section 9.2) dust could grow fast enough to restore a standard dust-to-gas ratio.

viii) It is difficult to predict the fraction of cold gas which is ionized by the galactic ionizing radiation. However, upper limits on the H_α radiation emitted by the off-center cold gas range from $\sim 5 \times 10^{37}$ to $\sim 10^{40}$, with the higher luminosity appropriate for the *CG* system.

ix) In the Appendix we show that the cold gas masses found in our simulations are likely overestimated by a factor of a few. This is due to numerical mixing and the following overcooling — a phenomenon important when small cold clouds move through a much hotter medium, sometimes overlooked in the literature.

REFERENCES

Alatalo K., Davis T. A., Bureau M., Young L. M., Blitz L., Crocker A. F., Bayet E., Bois M., Bournaud F., Cappellari M., Davies R. L., de Zeeuw P. T., Duc P.-A., Emsellem E., Khochfar S., Krajnović D., Kuntschner H., Lablanche P.-Y., Morganti R., McDermid R. M., Naab T., Oosterloo T., Sarzi M., Scott N., Serra P., Weijmans A.-M., 2013, MNRAS, 432, 1796

Balbus S. A., 1988a, ApJ, 328, 395

—, 1988b, ApJ, 328, 395

Balbus S. A., Soker N., 1989a, ApJ, 341, 611

—, 1989b, ApJ, 341, 611

Binney J., Nipoti C., Fraternali F., 2009, MNRAS, 397, 1804

Blanton E. L., Randall S. W., Clarke T. E., Sarazin C. L., McNamara B. R., Douglass E. M., McDonald M., 2011, ApJ, 737, 99

Bodo G., Ferrari A., Massaglia S., Rosner R., 1987, ApJ, 313, 432

Brighenti F., Mathews W. G., 1996, ApJ, 470, 747

—, 1997a, ApJ, 490, 592

—, 1997b, ApJ, 490, 592

—, 1999, ApJ, 512, 65

—, 2002, ApJ, 573, 542

—, 2006, ApJ, 643, 120

Buote D. A., Brighenti F., Mathews W. G., 2004, ApJ, 607, L91

Buote D. A., Lewis A. D., Brighenti F., Mathews W. G., 2003, ApJ, 594, 741

Caon N., Macchetto D., Pastoriza M., 2000, ApJS, 127, 39

Cavagnolo K. W., Donahue M., Voit G. M., Sun M., 2008, ApJ, 683, L107

Cazaux S., Spaans M., 2009, A&A, 496, 365

Cicone C., Maiolino R., Sturm E., Graciá-Carpio J., Feruglio C., Neri R., Aalto S., Davies R., Fiore F., Fischer J., García-Burillo S., González-Alfonso E., Hailey-Dunsheath S., Piconcelli E., Veilleux S., 2014, A&A, 562, A21

Ciotti L., D'Ercole A., Pellegrini S., Renzini A., 1991, ApJ, 376, 380

Costa T., Sijacki D., Haehnelt M., 2014, ArXiv e-prints

Cowie L. L., Fabian A. C., Nulsen P. E. J., 1980, MNRAS, 191, 399

Cox D. P., 2005, ARA&A, 43, 337

Dalgarno A., McCray R. A., 1972, Annual Review of Astronomy and Astrophysics, 10, 375

David L. P., Jones C., Forman W., Nulsen P., Vrtilek J., O'Sullivan E., Giacintucci S., Raychaudhury S., 2009, ApJ, 705, 624

David L. P., Lim J., Forman W., Vrtilek J., Combes F., Salome P., Edge A., Jones C., Sun M., O'Sullivan E., Gastaldello F., Temi P., Schmitt H., Ohyama Y., Hamer S., Mathews W., Brighenti F., Giacintucci S., Bardelli S., Trung D.-V., 2014, ArXiv e-prints

Davis T. A., Alatalo K., Sarzi M., Bureau M., Young L. M., Blitz L., Serra P., Crocker A. F., Krajnović D., McDermid R. M., Bois M., Bournaud F., Cappellari M., Davies R. L., Duc P.-A., de Zeeuw P. T., Emsellem E., Khochfar S., Kuntschner H., Lablanche P.-Y., Morganti R., Naab T., Oosterloo T., Scott N., Weijmans A.-M., 2011, MNRAS, 417, 882

de Plaa J., Zhuravleva I., Werner N., Kaastra J. S., Churazov E., Smith R. K., Raassen A. J. J., Grange Y. G., 2012, A&Ap, 539, A34

Donahue M., Voit G. M., 1993, ApJ, 414, L17

Draine B. T., Salpeter E. E., 1979, ApJ, 231, 77

Dwek E., 1988, ApJ, 329, 814

—, 1998, ApJ, 501, 643

Dwek E., Rephaeli Y., Mather J. C., 1990, ApJ, 350, 104

Ellis S. C., O'Sullivan E., 2006, MNRAS, 367, 627

Faber S. M., Tremaine S., Ajhar E. A., Byun Y.-I., Dressler A., Gebhardt K., Grillmair C., Kormendy J., Lauer T. R., Richstone D., 1997, AJ, 114, 1771

Fabian A. C., 2012, ARA&A, 50, 455

Gaspari M., Brighenti F., D'Ercole A., Melioli C., 2011a, MNRAS, 415, 1549

Gaspari M., Brighenti F., Temi P., 2012a, MNRAS, 424, 190

Gaspari M., Melioli C., Brighenti F., D'Ercole A., 2011b, MNRAS, 411, 349

Gaspari M., Ruszkowski M., Oh S. P., 2013, MNRAS, 432, 3401

Gaspari M., Ruszkowski M., Oh S. P., Brighenti F., Temi P., 2014, ArXiv e-prints

Gaspari M., Ruszkowski M., Sharma P., 2012b, ApJ, 746, 94

Gastaldello F., Buote D. A., Temi P., Brighenti F., Mathews W. G., Ettori S., 2009, ApJ, 693, 43

Goudfrooij P., Trinchieri G., 1998, A&A, 330, 123

Hattori M., Habe A., 1990, MNRAS, 242, 399

Hensley B. S., Ostriker J. P., Ciotti L., 2014, ApJ, 789, 78

Hirashita H., 2012, MNRAS, 422, 1263

Hirashita H., Kuo T.-M., 2011, MNRAS, 416, 1340

Joung M. R., Bryan G. L., Putman M. E., 2012, ApJ, 745, 148

Kaviraj S., Peirani S., Khochfar S., Silk J., Kay S., 2009, MNRAS, 394, 1713

Kaviraj S., Schawinski K., Devriendt J. E. G., Ferreras I., Khochfar S., Yoon S.-J., Yi S. K., Deharveng J.-M., Boselli A., Barlow T., Conrow T., Forster K., Friedman P. G., Martin D. C., Morrissey P., Neff S., Schiminovich D., Seibert M., Small T., Wyder T., Bianchi L., Donas J., Heckman T., Lee Y.-W., Madore B., Milliard B., Rich R. M., Szalay A., 2007, ApJS, 173, 619

Kim D.-W., Fabbiano G., 2004, ApJ, 611, 846

Koyama H., Inutsuka S.-i., 2004, ApJ, 602, L25

Lagos C. d. P., Padilla N. D., Davis T. A., Lacey C. G., Baugh C. M., Gonzalez-Perez V., Zwaan M., Contreras S., 2014, ArXiv e-prints

Lauer T. R., Faber S. M., Gebhardt K., Richstone D., Tremaine S., Ajhar E. A., Aller M. C., Bender R., Dressler A., Filippenko A. V., Green R., Grillmair C. J., Ho L. C., Kormendy J., Magorrian J., Pinkney J., Siopis C., 2005, AJ, 129, 2138

Li Y., Bryan G. L., 2014, ApJ, 789, 153

Loewenstein M., 1989a, MNRAS, 238, 15

—, 1989b, MNRAS, 238, 15

Loewenstein M., Mathews W. G., 1987, ApJ, 319, 614

Macchetto F., Pastoriza M., Caon N., Sparks W. B., Giavalisco M., Bender R., Capaccioli M., 1996, A&AS, 120, 463

Malagoli A., Rosner R., Bodo G., 1987a, ApJ, 319, 632

—, 1987b, ApJ, 319, 632

Malagoli A., Rosner R., Fryxell B., 1990a, MNRAS, 247, 367

—, 1990b, MNRAS, 247, 367

Martel A. R., Ford H. C., Bradley L. D., Tran H. D., Menanteau F., Tsvetanov Z. I., Illingworth G. D., Hartig G. F., Clampin M., 2004, AJ, 128, 2758

Mathews W. G., 1990, ApJ, 354, 468

Mathews W. G., Baker J. C., 1971, ApJ, 170, 241

Mathews W. G., Bregman J. N., 1978, ApJ, 224, 308

Mathews W. G., Brighenti F., 2003a, ARA&A, 41, 191

—, 2003b, ApJ, 590, L5

—, 2008, ApJ, 676, 880

Mathews W. G., Loewenstein M., 1986, ApJ, 306, L7

Mathis J. S., Rumpl W., Nordsieck K. H., 1977, ApJ, 217, 425

McCourt M., Sharma P., Quataert E., Parrish I. J., 2012, MNRAS, 419, 3319

McNamara B. R., Nulsen P. E. J., 2007, ARA&A, 45, 117

Mellier Y., Mathez G., 1987, A&A, 175, 1

Mulchaey J. S., Jeltema T. E., 2010, ApJ, 715, L1

Navarro J. F., Frenk C. S., White S. D. M., 1996, ApJ, 462, 563

Panagoulia E. K., Fabian A. C., Sanders J. S., Hlavacek-Larrondo J., 2014, ArXiv e-prints

Parriott J. R., Bregman J. N., 2008, ApJ, 681, 1215

Pizzolato F., Soker N., 2005, ApJ, 632, 821

—, 2010, MNRAS, 408, 961

Reale F., Rosner R., Malagoli A., Peres G., Serio S., 1991, MNRAS, 251, 379

Rebusco P., Churazov E., Böhringer H., Forman W., 2006, MNRAS, 372, 1840

Revaz Y., Combes F., Salomé P., 2008, A&A, 477, L33

Sanders J. S., Fabian A. C., Smith R. K., 2011, MNRAS, 410, 1797

Sarzi M., Alatalo K., Blitz L., Bois M., Bournaud F., Bureau M., Cappellari M., Crocker A., Davies R. L., Davis T. A., de Zeeuw P. T., Duc P.-A., Emsellem E., Khochfar S., Krajnović D., Kuntschner H., Lablanche P.-Y., McDermid R. M., Morganti R., Naab T., Oosterloo T., Scott N., Serra P., Young L. M., Weijmans A.-M., 2013, MNRAS, 432, 1845

Sarzi M., Falcón-Barroso J., Davies R. L., Bacon R., Bureau M., Cappellari M., de Zeeuw P. T., Emsellem E., Fathi K., Krajnović D., Kuntschner H., McDermid R. M., Peletier R. F., 2006, MNRAS, 366, 1151

Serra P., Oosterloo T., Morganti R., Alatalo K., Blitz L., Bois M., Bournaud F., Bureau M., Cappellari M., Crocker A. F., Davies R. L., Davis T. A., de Zeeuw P. T., Duc P.-A., Emsellem E., Khochfar S., Krajnović D., Kuntschner H., Lablanche P.-Y., McDermid R. M., Naab T., Sarzi M., Scott N., Trager S. C., Weijmans A.-M., Young L. M., 2012, MNRAS, 422, 1835

Serra P., Oser L., Krajnović D., Naab T., Oosterloo T., Morganti R., Cappellari M., Emsellem E., Young L. M., Blitz L., Davis T. A., Duc P.-A., Hirschmann M., Weijmans A.-M., Alatalo K., Bayet E., Bois M., Bournaud F., Bureau M., Crocker A. F., Davies R. L., de Zeeuw P. T., Khochfar S., Kuntschner H., Lablanche P.-Y., McDermid R. M., Sarzi M., Scott N., 2014, MNRAS, 444, 3388

Sharma P., McCourt M., Quataert E., Parrish I. J., 2012, MNRAS, 420, 3174

Simões Lopes R. D., Storchi-Bergmann T., de Fátima Saraiva M., Martini P., 2007, ApJ, 655, 718

Singh A., Sharma P., 2015, MNRAS, 446, 1895

Smith M. W. L., Gomez H. L., Eales S. A., Ciesla L., Boselli A., Cortese L., Bendo G. J., Baes M., Bianchi S., Clemens M., Clements D. L., Cooray A. R., Davies J. I., de Looze I., di Serego Alighieri S., Fritz J., Gavazzi G., Gear W. K., Madden S., Mentuch E., Panuzzo P., Pohlen M., Spinoglio L., Verstappen J., Vlahakis C., Wilson C. D., Xilouris E. M., 2012, ApJ, 748, 123

Spitzer L., 1978, Physical processes in the interstellar medium

Stone J. M., Norman M. L., 1992, ApJs, 80, 753

Sutherland R. S., Dopita M. A., 1993, ApJS, 88, 253

Tadhunter C., Morganti R., Rose M., Oonk J. B. R., Oosterloo T., 2014, Nature, 511, 440

Temi P., Brighenti F., Mathews W. G., 2007, ApJ, 666, 222

—, 2009, ApJ, 695, 1

Temi P., Brighenti F., Mathews W. G., Bregman J. D., 2004, ApJS, 151, 237

Temi P., Mathews W. G., Brighenti F., Bregman J. D., 2003, ApJl, 585, L121

Thom C., Tumlinson J., Werk J. K., Prochaska J. X., Oppenheimer B. D., Peeples M. S., Tripp T. M., Katz N. S., O'Meara J. M., Ford A. B., Davé R., Sembach K. R., Weinberg D. H., 2012, ApJ, 758, L41

Trager S. C., Faber S. M., Worthey G., González J. J., 2000, AJ, 120, 165

Tran H. D., Tsvetanov Z., Ford H. C., Davies J., Jaffe W., van den Bosch F. C., Rest A., 2001, AJ, 121, 2928

Trinchieri G., Goudfrooij P., 2002, A&A, 386, 472

Trinchieri G., Noris L., di Serego Alighieri S., 1997, A&A, 326, 565

Tsai J. C., Mathews W. G., 1995, ApJ, 448, 84

—, 1996, ApJ, 468, 571

Voit G. M., Cavagnolo K. W., Donahue M., Rafferty D. A., McNamara B. R., Nulsen P. E. J., 2008, ApJ, 681, L5

Werner N., Oonk J. B. R., Canning R. E. A., Allen S. W., Simionescu A., Kos J., van Weeren R. J., Edge A. C., Fabian A. C., von der Linden A., Nulsen P. E. J., Reynolds C. S., Ruszkowski M., 2013, ApJ, 767, 153

Werner N., Oonk J. B. R., Sun M., Nulsen P. E. J., Allen S. W., Canning R. E. A., Simionescu A., Hoffer A., Connor T., Donahue M., Edge A. C., Fabian A. C., von der Linden A., Reynolds C. S., Ruszkowski M., 2014, MNRAS, 439, 2291

Werner N., Zhuravleva I., Churazov E., Simionescu A., Allen S. W., Forman W., Jones C., Kaastra J. S., 2009, MNRAS, 398, 23

Young L. M., Bureau M., Davis T. A., Combes F., McDermid R. M., Alatalo K., Blitz L., Bois M., Bournaud F., Cappellari M., Davies R. L., de Zeeuw P. T., Emsellem E., Khochfar S., Krajnović D., Kuntschner H., Lablanche P.-Y., Morganti R., Naab T., Oosterloo T., Sarzi M., Scott N., Serra P., Weijmans A.-M., 2011, MNRAS, 414, 940

Zhukovska S., Gail H.-P., Trieloff M., 2008, A&Ap, 479, 453

APPENDIX A: NUMERICAL MIXING AND OVERCOOLING

Numerical mixing at the interfaces between cold and hot gas can cause large errors in the computed cooling rate — not always recognized in the literature. This is especially true when the cold gas clouds are resolved in only a few zones and when the difference in temperature and density between the two phases is sizable. These are exactly the circumstances of our simulations, where small blobs of $T \lesssim 10^4$ K gas move through $\sim 10^7$ K hot atmosphere. Numerical averaging at the surfaces separating cold and hot gas results in zones of gas at intermediate density and temperature. Radiative cooling can be either overestimated and underestimated, depending on the flow parameters, with the former case dominating in our simulations. Brighenti, Mathews & Temi (2014) also discuss the magnitude of this errors in simulations similar to those presented here. They argue that adding a temperature dependent "dropout" term to the continuity equation, which removes from the grid the currently cooling gas, largely reduces the spurious overcooling. The trade off of this procedure is, of course, the inability to follow the subsequent dynamics of the cooled gas; only its amount and the location of its formation can be estimated. This term has already been introduced in Section 2.2.2, see Brighenti, Mathews & Temi (2014) for more details. The term added to the continuity equation reads:

$$\left(\frac{\partial \rho}{\partial t}\right)_{\rm do} = -q(T)\frac{\rho}{t_{\rm cool}}; \quad q(T) = q_0 \exp\left[-(T/T_c)^2\right] \quad \text{(A1)}$$

and a corresponding term is needed to the energy equation (see Brighenti, Mathews & Temi 2014). Here we choose $T_c = 5 \times 10^5$ K. These dropout terms are negligibly for $T \gtrsim T_c$. By targeting only gas with $T \lesssim T_c$ means that we remove gas that is currently cooling and will reach $T \lesssim 10^4$ K in a very short time. That is why this method produces accurate cooling (dropping out) rates, providing $T_c \lesssim 10^6$ K (see Brighenti & Mathews 2002). The precise value of q_0 hardly matters and we choose $q_0 = 2$ to match our previous calculations.

Needless to say, this technique to alleviate numerical overcooling is not perfect. A sensible way to gauge the magnitude of this error is to calculate similar models with and without the dropout term (acting in the whole numerical grid), and compare the amount of cooled (dropped out) gas
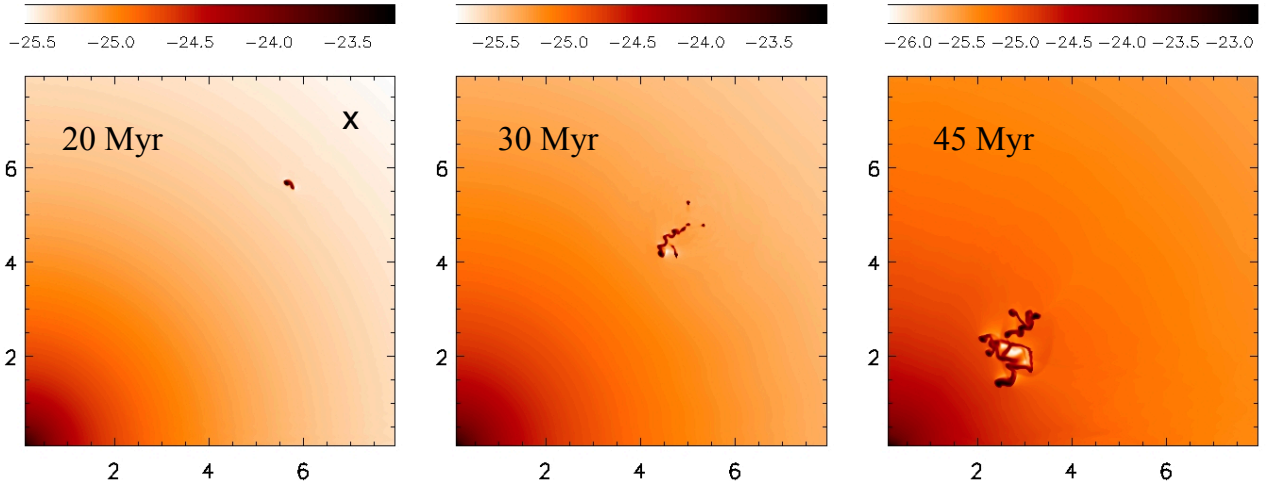
Figure A1. *Left column:* density maps for the "one-zone" experiment at three different times. In the left panel the "x" indicates the original location of the single cold zone. The z-axis is horizontal, the R-axis is vertical. Units are kpc. It is evident that the small cloud induces a "snowball" cooling effect as it moves through the grid. Notice that the color scale differs for every panel.

in the two cases; the physical truth lies in between these two extrema, with the dropout value likely to be more accurate.

A1   "One cold zone" experiment

Before to make this comparison for the CG model, we show with a suite of idealized, somewhat pedantic, numerical experiments the occurrence and the effect of the overcooling. We follow the evolution of a one-zone cold cloud, located in the same gas atmosphere of the CG model at $(R, z) = (7, 7)$ kpc. The temperature of the zone is set to 10^4 K and its density is calculated assuming pressure equilibrium with the surrounding hot gas. The numerical resolutions adopted for the calculations are $\Delta R = \Delta z = 20$ or 10 pc. The dropout term above is not used in this experiment, and the cold gas is simply advected under gravity toward the galaxy center. The cloud evolution for the radiative case, resolution 20 pc, is shown in Figure A1.

At $t = 20$ Myr the mass of the cloud has grown by a factor 2.4, as can be seen in Figure A2 (solid line), where we show the cold gas mass evolution (normalized to the initial cold mass). This increase in the cold gas mass is spurious and it is due to numerical overcooling. While this mimics some physical processes (for example the condensation for clouds larger than the Field length, when thermal conduction is present), we stress that in the hydrodynamical equations solved no transport terms (which deal with microscopic fenomena such as diffusion) are present, therefore any increment of the cold gas mass must be regarded as spurious. At the end of the calculation (50 Myr), the cold gas has grown by a factor $\gtrsim 40$.

If the radiative cooling is turned off, numerical mixing consumes the cold cloud, in a time $t \sim 10$ Myr (Figure A2, dashed line). After this time the original cloud gas has been mixed with hot gas and raised its temperature to values $> 5 \times 10^5$ K, our threshold for the definition of cold gas.

We run two more simulations at higher resolution (10 pc). The first shows that a (radiative) single zone cloud in-

creases its mass by a factor $\gtrsim 100$ (Figure A2, dotted line). In the second, high resolution experiment we consider a 4-zones cloud (which is then physically identical to the single-zone cloud at 20 pc resolution). In this case, illustrated in Figure A2 with a long-dashed line, the cold gas mass growth is almost identical to the model described by the solid line. This implies that a modest increase in the numerical resolution likely does not solve the numerical mixing problem.

These few simple calculations, although extreme, are relevant for our calculations. It is our experience that regions of cold ($\sim 10^4$ K) gas only one or a few zones across can arise naturally in radiating gas dynamics (Koyama & Inutsuka 2004). Thus, small elements of cold gas can trigger large unintended numerical overcooling due to unphysical mixing with much hotter gas. Conversely, in very slowly cooling or adiabatic flows, some degree of numerical overheating can occur. The physical truth lies between these two extremes.

A2   Numerical overcooling in the CG-FB models

In this section we address the effect of numerical overcooling in some CG-FB models. We also performed experiments for IG-FB calculations, with similar results. For the sake of conciseness, we present results for only two runs of CG-FB with jet velocities $v_{\rm jet} = 4000$ and 16000 km s^{-1}. These calculations are identical to those described in Section 5.1, but the term in equation A1 (and an analogue term in the energy equation) is activated on the whole numerical grid. In Figure A3 we show the cumulative mass dropped out in the off-center region and compare it with the cold gas mass found in the same region for the respective standard models (see Section 5.1). The masses which are portrayed in Figure A3 have different meaning. For the standard models, the displayed mass represents the instantaneous cold gas mass present in the off-center region: this cold gas then flows toward the center, disappearing from that region. For the dropout runs it is instead the total gas mass which has
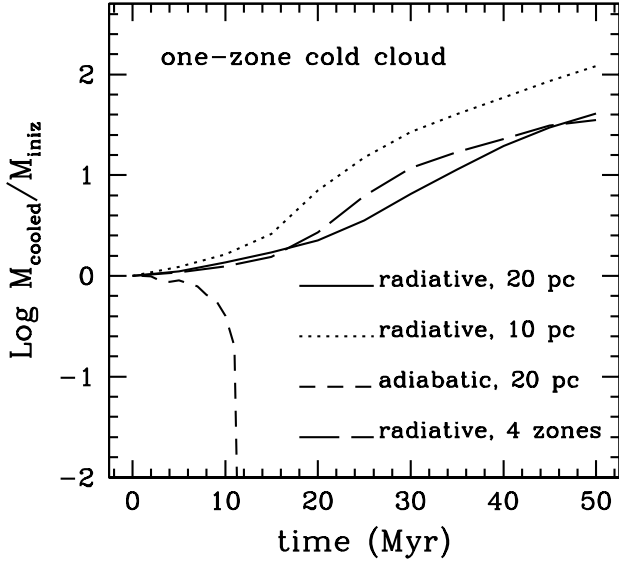
Figure A2. Time evolution of the cold gas mass for the one-zone (and one four-zones) experiments. For every run the mass is normalized to the initial cold mass. In radiative simulations numerical mixing causes overcooling, while in the adiabatic calculation the spurious mixing erases the cloud in a short time.
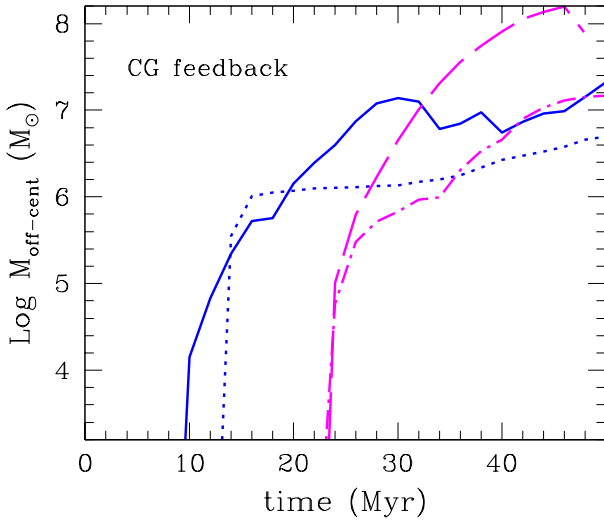
Figure A3. Time evolution of the cold gas mass for two *CG-FB* models. The solid blue line indicates the same *CG-FB4000* model shown in Figure 8. In this calculation no dropout term has been used. The blue dotted line represents the same model, but with the term A1 adopted. The two magenta lines show the standard (dashed line) and the dropout (dot-dashed) version of *CG-FB16000*.

$(R, z) \approx (1.5, 4)$ kpc. These blobs, initially only a few tens pc in size, grow in size and mass by numerical mixing as they move through the grid, exactly as depicted in Figure A1. That is, overcooling has been triggered. The mass discrepancy can be as large as one order of magnitude, and will be not reduced by increasing the numerical resolution by a factor of a few. Therefore, the cold gas mass values quoted in the previous sections are uncertain by (at least) a factor of a few. Although we argue that the dropout masses are closer to the physical truth than the cold gas masses calculated in the standard fashion, we focused on the latter estimates in the text, mostly for the sake of tradition. However, we stress the need to evaluate, whenever possible, the uncertainty in the cooling gas mass due to numerical overcooling, using a drop out procedure or other appropriate experiments.

been cooled and removed from the grid since $t = 0$. That is why it is a monotonically increasing value.

The effect of the overcooling in the case of no-dropout is clear, especially for the $v_{\rm jet} = 16000$ km s^{-1} model. In the temperature map, not shown here, it is evident as a large number of small cold blobs form at $t \sim 25$ Myr for